Carbon 226 (2024) 119221

Contents lists available at ScienceDirect

Carbon

journal homepage: www.elsevier.com/locate/carbon

Conversion of biodigestate into activated carbon for electrochemical application: Process performance and life cycle assessment

Elisabetta Petri [a,1], Eva-Maria Heigl [b,1,**], Andrea Fasolini [c,d], Lukas Zeilerbauer [b,e,f], Monica Giovannucci [a], Yusuf Küçükağa [a], Cristian Torri [a], Francesco Basile [c,d], Francesca Soavi [a,g,*]

[a] Department of Chemistry "Giacomo Ciamician", Alma Mater Studiorum University of Bologna, Via Selmi 2, 40126, Bologna, Italy
[b] Energieinstitut an der Johannes Kepler Universität Linz, Altenberger Straße 69, 4040, Linz, Austria
[c] Department of Industrial Chemistry "Toso Montanari", University of Bologna, Viale Risorgimento, 4, 40136, Bologna, Italy
[d] Center for Chemical Catalysis - C3, University of Bologna, Viale Risorgimento, 4, 40136, Bologna, Italy
[e] Institute for Chemical Technology of Organic Materials (CTO), Johannes Kepler University Linz, Altenberger Straße 69, 4040, Linz, Austria
[f] Institute of Polymeric Materials and Testing (IPMT), Johannes Kepler University Linz, Altenberger Straße 69, 4040, Linz, Austria
[g] Center for the Environment, Energy, and Sea - Interdepartmental Centre for Industrial Research in Renewable Resources, Environment, Sea and Energy (CIRI-FRAME), Alma Mater Studiorum University of Bologna Viale Ciro Menotti, 48, 48122, Marina di Ravenna, RA, Italy

ARTICLE INFO

Keywords:
Activated biochar
Lignin
Pyrolysis
Life cycle assessment
Anaerobic digestate
Supercapacitors

ABSTRACT

Carbons derived from pyrolysis and activation of waste biomass are attracting much attention as components of energy technologies, such as batteries, supercapacitors and fuel cells. This experimental study focuses on the production of a high-surface-area biochar (LAC) obtained from the treatment of lignin-rich waste of a biodigester plant, by applying $KHCO_3$ as an activating agent. The pyrolysis-activation conditions were set by following the process by thermogravimetric analysis and by checking the purity and porosity of the resulting carbon by several analytical techniques. The best pyrolysis condition provided a microporous carbon featuring up to 1840 $m^2\ g^{-1}$, which was demonstrated at a 25 g biodigestate batch-scale. Moreover, the production process was critically analyzed by means of life cycle assessment to identify environmental hotspots and thus derive recommendations for process optimization. The impact of substance- and energy-recovery and the use of renewable energy sources on the sustainability of the product was demonstrated in several scenarios, complemented by benchmarking and an outlook regarding further optimization needs. In the best case scenario, the global warming potential of the proposed biochar could be reduced to 15.9 kg CO_2-eq per kg of LAC. The activating agent $KHCO_3$ was dominant in almost all environmental impact categories, hence, a theoretical recovery process for this substance was suggested and evaluated via life cycle assessment.

1. Introduction

Electrochemical energy storage and conversion devices have a tremendous impact on the energy transition pathway towards a decarbonized society. Batteries, supercapacitors, fuel cells and electrolyzers are considered to be the most efficient technologies for renewable energy management, conversion and storage. Different forms of carbon are present in all these systems and are selected, processed and modified differently, according to their application [1]. Carbon is a strategic element, possessing desirable characteristics such as high electrical conductivity, abundance on earth, cost-effectiveness and high stability in various electrolytes including aqueous and organic solutions. These features enable carbon exploitation for different uses: to improve the conductivity of electrodes, to store charge (by ion capacitive adsorption or faradaic insertion), and to promote electrocatalytic processes. Furthermore, carbonaceous materials can be easily produced by pyrolysis of biomass from many renewable feedstocks and organic wastes (mainly from agriculture and food residues) [2]. Pyrolysis is a

* Corresponding author. Department of Chemistry "Giacomo Ciamician", Alma Mater Studiorum University of Bologna, Via Selmi 2, 40126, Bologna, Italy.
** Corresponding author.
E-mail addresses: heigl@energieinstitut-linz.at (E.-M. Heigl), francesca.soavi@unibo.it (F. Soavi).
[1] These authors contributed equally.

https://doi.org/10.1016/j.carbon.2024.119221
Received 19 February 2024; Received in revised form 26 April 2024; Accepted 6 May 2024
Available online 6 May 2024

thermochemical technology used to convert biomass into energy and chemical materials. The products are classified as liquid bio-oil, solid biochar, and pyrolytic gas (syngas) [3]. During biomass pyrolysis, many reactions occur in parallel and in series, including dehydration, depolymerization, isomerization, aromatization, decarboxylation, and carbonization (i.e. charring). Large-scale and low-cost production of biochar, derived from biomass [4–6], might contribute to the valorization of waste materials within a circular economy framework. Indeed, the manufacturing of energy technologies by exploiting waste-derived components such as biochar for batteries, supercapacitors and fuel cells perfectly addresses the 5 R principle (Reduce, Reuse, Recycle, Recover and Restore) that underpins the foundation of the waste-energy nexus [7]. Biomass utilization for energy technologies also supports several of the 17 Sustainable Development Goals (SDS) of the UN, such as SDG 7, which aims at ensuring "access to affordable, reliable, sustainable and modern energy for all" [8,9].

Biomass-based products can, under certain conditions, have a mitigating effect on climate change through the sequestration of CO_2 from the atmosphere and the substitution of fossil-based products with potentially higher CO_2 emissions, thus reducing further emissions. However, both effects need to be thoroughly evaluated in every case to avoid drawing incorrect conclusions. During growth, biomass removes CO_2 from the atmosphere and fixes the carbon in its structure. This is per se a carbon negative mechanism. However, when producing a product from biomass feedstock, the production process also causes CO_2 emissions, which may even exceed the amount sequestered by the biomass. Whether a biomass-based product causes positive, neutral or negative CO_2 emissions in its lifecycle depends on the aforementioned carbon balance and on the timeframe of the assessment: if long-term storage of the sequestered biogenic carbon can be achieved, the carbon uptake of the biomass may be considered a negative emission; if the carbon is released again to the atmosphere after a short period of time, for example through combustion processes, the carbon balance of short-term sequestering and releasing of biogenic CO_2 would be regarded as neutral. But even short-term removal and storage of atmospheric CO_2 can have a certain mitigating effect, as the stored carbon does not contribute to climate change during the storage period [10,11].

Recently, considerable effort has been devoted to refining the physicochemical properties of biochars, focusing on aspects such as their porous architecture, surface area, particle size, morphology, degree of graphitization, and surface decoration through functional groups and/or heteroatoms. Notably, these properties depend on the biomass feedstock and pyrolysis parameters, often including chemical and/or physical activation steps. The latter are mainly adopted to improve the specific surface area, which is especially important for the development of supercapacitors and electrocatalytic systems (fuel cells and electrolyzers) [12–16]. The progress in the use of biomass-derived carbons for electrochemical energy storage/conversion systems has been thoroughly reviewed by Escobar et al. (2021) [17]. In their work, the authors discussed the role of biomass precursors, pyrolysis methodologies and activation treatments for the production of biochar with desired textural properties and surface chemistries [17]. During pyrolysis, the biomass is carbonized in an inert atmosphere (e.g. under nitrogen) at high temperatures typically ranging from 600 to 900 °C. This process subjects the carbon-rich organic feedstock to heat treatment to eliminate the non-carbon elements. The resulting biochar typically has relatively low porosity, comprising elementary crystallites with a large number of interstices, often filled with "disorganized" carbon residues (tar). The activation process, which can be integrated into the pyrolysis step, opens the pores and creates additional porosity. There are two main routes to activate carbonaceous materials: physical and chemical activation, which use oxidizing gases or oxidizing agents (e.g. KOH, NaOH, $ZnCl_2$, H_3PO_4) [18–21].

In terms of precursors, lignin-rich biomass is expected to provide high a carbon yield due to its higher thermal stability compared to cellulose and hemicellulose [22,23]. Cellulose, hemicellulose and lignin constitute the majority of biogenic carbon sources [24–28]. In addition, lignin is emerging as a strategic resource, because it is the second most abundant compound, following cellulose, within the plant kingdom. It serves as a by-product of many important industrial sectors, ranging from the paper industry to biodigester plants. It is expected that by 2030 global lignin generation will surpass 225 million tons per year [29–31]. Lignin-rich source pyrolysis and activation have been thoroughly investigated and lignin-derived activated biochar has been proposed for supercapacitors and fuel cells [32–39]. Highly porous carbons have been derived from lignin-rich precursors using various chemical and physical activation processes [40]. Under appropriate activation conditions, it is possible to obtain materials with surface areas and pore volumes approaching 2000 $m^2\ g^{-1}$ and 1 $cm^3\ g^{-1}$, respectively. Relevant published data on the properties of activated chars from different lignocellulosic precursors are available in Refs. [40,41].

Potassium bicarbonate ($KHCO_3$), which is not classified as a hazardous substance according to the European CLP directive [42], is emerging as a chemical activating agent because of its less corrosive and more environmentally friendly behaviour, as compared to alkaline oxides [43–49]. Activated biochar using $KHCO_3$ from real lignin-rich biodigestate wastes (Lignin Activated Carbon - LAC) displays a specific surface area higher than 1800 $m^2\ g^{-1}$ [38]. In our previous works, we demonstrated that LAC can be used to produce electrodes for supercapacitors as well as inorganic and microbial fuel cells [38,39,50]. Notably, LAC features more than 100 F g^{-1} in aqueous electrolytes and enables the design of a supercapacitor with a specific energy of 10 Wh kg^{-1}. As an electrocatalyst, LAC features high electrochemical oxygen reduction reaction (ORR) activity, especially at high current densities in a neutral environment in an air-breathing microbial fuel cell. When functionalized by metals, such as iron and manganese, LAC is an excellent electrocatalyst for oxygen reduction in both proton-exchange-membrane and anion-exchange-membrane fuel cells [38,39].

Overall, LAC can be considered as a strategic material for the ecodesign of energy-related technologies in Europe. Indeed, as an example, today the activated carbon used for supercapacitor electrodes comes from resources that are located mainly outside Europe, such as coconut shells [51]. Hence, LAC offers the opportunity to exploit local and widespread biodigester wastes and transform them into valuable components in the energy storage/conversion supply chain. Biogas production is gaining increasing importance in the course of energy transition [52], with growing amounts of biodigestate to be expected in the future. Using local or regional precursors for production of activated carbon in Europe reduces the dependency on resources from other world regions and the need for transport over long distances. In addition, technology levels as well as environmental protection standards often are stricter in Europe than in other regions of the world.

With this view, in the recent European Project HyFlow, we aimed at exploiting LAC to develop a supercapacitor to be combined with a vanadium redox flow battery in a hybrid energy storage system for renewable energy plants [53]. Despite the preliminary evidence of the great potential of LAC for supercapacitor applications that was demonstrated at the small cell level, further assessment was required to evaluate its use in the HyFlow demonstrator, which would need a LAC amount in the kilogram scale. Specifically, a deeper analysis of the effect of the pyrolysis conditions on the carbon yield and porosity, as well as the identification of environmental hotspots of the LAC production process were needed. Indeed, to date, the production and electrochemical performance of this char have been demonstrated solely at the laboratory scale using batches of a few grams. Large-scale production plants are not available, yet. The engineering of LAC production requires great attention to pyrolysis and activation processes, which should be tailored considering the end-use of the biochar, in our case supercapacitor production.

Production yield and porous architecture of the biochar are key features for this use-case. In turn, they are affected by pyrolysis/

activation conditions. Indeed, during the high-temperature phase of the thermal activation, the oxidizing atmosphere generally increases the pore volume and surface area of the material by means of a controlled carbon "burn-off" with the elimination of volatile pyrolysis products. The level of burn-off is extremely important and is controlled by temperature: a high degree of activation is achieved by increased burn-off, which in turn lowers the production yield [54,55].

Hence, unlike in our previous work, that was mainly focused on the demonstration of LAC performance for specific applications, such as supercapacitors and fuel cells, here we focus on the evaluation of the biochar production process, in view of its upscaling. We deeply analyze the one-step pyrolysis/$KHCO_3$-activation of LAC from real biodigester waste, focusing on the effect of time and temperature on production yield and carbon porosity, as well as on the evaluation of the energy content of pyrolysis by-products. By taking into account data collected by thermogravimetric analysis on the milligram scale, we define production protocols that we applied to the pyrolysis of small (7 g-scale) and larger (25 g-scale) batches. The porous architecture of the produced biochars was evaluated by N_2-adsorption porosimetry, scanning electron microscopy (SEM) and transmission electron microscopy (TEM). Raman spectroscopy and X-ray Diffraction (XRD) were used to get insight into LAC graphitization. In parallel, quantitative pyrolysis-activation analysis provided important information on the energy content of the by-products, allowing for the development of possible valorization strategies.

In the second part of this study, the suggested LAC production process was critically evaluated from an environmental perspective through life cycle assessment (LCA). Even if benchmarking of a new product or process that is still under development with comparable (commercial) products is of high interest to stakeholders, the main and most sensible goal of LCA of a process at a low technology readiness level usually is the identification of environmental hotspots, thus deriving potentials for environmentally-targeted process optimization [56]. Based on the results of the hotspot analysis of the LAC production process, various scenarios were assessed to demonstrate the influence of substance- and energy-recovery, along with the utilization of renewable energy sources on the sustainability of the product. Special caution is required when comparing a process at a low technology readiness level to a process at a high technology readiness level or to a proven industrial process, such as industrial AC from hard-coal, by means of life cycle assessment, as this can easily lead to misinterpretations due to scaling effects and possible future process changes and developments [56]. To allow for a more robust benchmarking, the suggested LAC production process was upscaled from a gram to a kilogram batch-scale by applying the methodology developed by Picchinno et al. (2016) [57] for LCA of chemical processes. However, various limitations of benchmarking still remain in our case and were thoroughly discussed in this publication.

No LCA of a bio-based AC production process for electrochemical application with $KHCO_3$ as activating agent, which could serve as a direct reference, was found in literature; however, there exists a number of LCA studies on bio-based AC applying other activating agents, including steam [58], H_3PO_4 [59,60], $ZnCl_2$ [59] or, most common for chemical activation [61], KOH [62]. Wang et al. (2022) [62], who applied KOH, found that this activating agent causes a large share of the environmental impacts of the AC production process, especially regarding the global warming potential (GWP). They also showed that recycling of KOH from process waste water and thus avoiding the disposal of hazardous waste, would have the potential to significantly lower GWP emissions of the AC production process. However, they chose a simplified approach for their recycling scenario by applying an assumed recycling rate of 90 % [62]. Montes and Hill (2018) [61] have already demonstrated that, in fact, KOH can be recovered from activation waste water, but did not investigate their recycling process with LCA. Based on this literature research, we assumed that $KHCO_3$ would also have a high environmental impact on the LAC production process, requiring the development of possible mitigation strategies.

2. Experimental details

This section describes the investigated LAC production process and the methodologies applied for laboratory analyses and LCA.

2.1. Lignin-derived biochar production

The biochar precursor was a solid waste (not digested quote) derived from an anaerobic biodigester plant (Biotech Sys. S.r.l., Bologna) fed with energy crops (corn and wheat silages) and a minor quote of dung. As with any waste material, biodigestate composition can vary, potentially affecting biochar yield and morphology. To simplify our study and minimize variability, we utilized the same identical sample of biodigestate source for producing the various biochars. The biodigestate was washed with a water/ethanol mixture, dispersed in an aqueous solution with a mild activating agent ($KHCO_3$), and pyrolyzed at 800 °C or 900 °C for 1 h or at 850 °C for 30 min under nitrogen. The resulting biochar underwent sieving, deashing with 3 M HCl and washing. A detailed description of the materials and processes used to prepare the batch for subsequent pyrolysis is reported in Section 3.1.2 and in the Supplementary Information file and is summarized in Table S1. Table 1 reports the codes for the different pyrolyzed batches, along with their pyrolysis conditions.

The pyrolysis process was followed by thermogravimetric analysis (TGA) and quantitative pyrolysis (hereinafter bench-scale pyrolysis) of the impregnated biodigestate. TGA was performed by TA instrument TGA Q50. Both argon and oxygen flowed continuously during the analysis at flow rates of 40 mL min^{-1} and 60 mL min^{-1}, respectively. Quantitative pyrolysis was conducted by mimicking the operational conditions of the pyrolysis/activation tests previously explained above (5 °C min^{-1} to 850 °C under continuous N_2) [63,64]. Each product resulting from quantitative pyrolysis was collected separately [63,64] to determine the mass yields of the pyrolysis products. After bench-scale pyrolysis, solid biochar, potash-glass and liquid bio-oil portions were recovered, weighed and analyzed. The gas fraction (known as pyrolytic gas or syngas) was collected in a laminated gasbag (Supel™-Inert Multi-Layer Foil), volumetrically measured, and analyzed using a gas-chromatography (GC) system equipped with a thermal capture detector (TCD) to quantify the fractions of H_2, CH_4, CO_2, CO and N_2. Subsequently, the mass of the gas portion was calculated by multiplying the gas volume with the gas density at room temperature (RT) and pressure.

2.2. Chemical-physical characterization

Nitrogen adsorption porosimetry analysis was performed to investigate the textural properties of the produced biochar. After drying for 24 h at 413 K, measurements were carried out at 77 K, using ASAP 2020 system (Micromeritics). The specific surface area (S_{BET}) and pores size distribution (PSD) were quantified using the Brunauer-Emmett-Teller (BET) and density functional theories (DFT). Morphological features and chemical composition of the samples were studied using scanning electron microscopy (SEM, Zeiss EVO 50 microscope) equipped with an energy-dispersive X-ray analyzer (EDS, Oxford INCA Energy 350

Table 1
Codes and pyrolysis conditions of the LAC batches.

Sample	Mass of biodigestate	Mass of $KHCO_3$	Pyrolysis conditions
B7.1	12 g	24 g	Ramp 5 °C min^{-1} to 850 °C Isothermal at 850 °C for 30′
B7.2	7.7 g	15.4 g	Ramp 5 °C min^{-1} to 900 °C Isothermal at 900 °C for 60′
B7.3	7 g	14 g	Ramp 5 °C min^{-1} to 800 °C Isothermal at 800 °C for 60′
B17	24.3 g	48.7 g	Ramp 5 °C min^{-1} to 850 °C Isothermal at 850 °C for 30′

system). Raman analysis was performed using a micro-spectrometer Renishaw Raman RM1000 connected to a Leica microscope DMLM (obj. 5 × , 20 × . 50 ×). The available source was an Ar^+ laser (λ = 514.5 nm). The system was supplemented with a notch filter for the Ar^+ laser to eliminate Rayleigh scattering. The instrument was equipped with a charge-coupled device detector with thermo-electrical cooling (203 K). X-ray diffraction (XRD) analysis was performed to obtain diffractogram patterns. The results were obtained using a PanAnalytical X'Pert apparatus with a copper target and nickel filter in the 10 °–60° 2θ range and using an X'Celerator detector at 40 kV and 40 kA. Transmission electron microscopy (TEM) images were obtained using a Philips CM100 (accelerating voltage 80 kV), and deionised millipore H_2O was used as a dispersing agent for the preparation of TEM carbon samples.

The electrochemical behaviour of the biochar was evaluated by cyclic voltammetry in 6 M KOH. Single electrode tests were carried out using single-coated AC electrodes with Nickel foam as the current collector. The results were compared with those obtained with commercial carbon (PICA BP10). The electrode materials were prepared by mixing the active material (PICA or LAC), SUPER C65 Conductive Carbon Black (C65, Imerys) and polyvinylidene fluoride at a ratio of 8:1:1, followed by the addition of N-methyl-2-pyrrolidone (NMP) solution to form a slurry. The slurry was coated onto the prepared Ni-foam and dried at 60 °C overnight. A Biologic VSP multichannel potentiostat/galvanostat was used. Cyclic Voltammetries (CVs) were run at room temperature (RT) at 10 mV s^{-1}.

2.3. Life cycle assessment

To evaluate the environmental impacts caused by the production phase of LAC, a cradle-to-gate LCA following the four phases of ISO 14040/14044 LCA standards [65,66] was conducted: definition of goal and scope, life cycle inventory (LCI), life cycle impact assessment (LCIA) and improvement and interpretation. By defining the goal and scope, the further design of the LCA study is framed and expectations of all involved parties are aligned. Subsequently, the LCI is created by compiling information on process inputs and outputs and performing mass- and energy-balances. The results of the LCI analysis are then transferred into environmental impacts in a step called LCIA by applying harmonized LCIA methodologies. And finally, LCIA results are discussed and complemented by a sensitivity analysis and an overview of the limitations and weaknesses of the study. The process of LCA is iterative, ensuring a continuous alignment between the different steps and an adaption of these if necessary [65–70]. For more information on the applied LCA methodology, standard works such as the ones by Frischknecht et al. (2020) [67], Guinée et al. (2002) [68], Curran (Ed.) (2014) [69] or Klöpffer and Grahl (2014) [70] are recommended.

2.3.1. Goal, scope and functional unit

The goal of this LCA study was to perform a cradle-to-gate LCA of the here suggested LAC production process, with the discussion focusing on climate change (resp. GWP), followed by benchmarking with other AC products. As the LAC production still is in an early development phase, environmental hotspots in the suggested production process should be identified, thus deriving recommendations for process optimization. The scope of this LCA comprised the steps of biomass-farming, anaerobic digestion, transport and LAC production through pyrolysis, activation and purification. Environmental impacts inferred by the use and disposal of the LAC were not assessed. The production of the LAC and its precursor took place in Italy, therefore the geographical system boundary was defined as Europe. The functional unit of this LCA is 1 kg of produced LAC.

2.3.2. Life cycle inventory

LCI data were mainly derived from the suggested laboratory-scale LAC production process and complemented by datasets from LCA databases and valid literature sources. Laboratory-scale process data were upscaled applying the framework of Piccinno et al. (2016) [57] for LCA of chemical processes. For LCA modelling GaBi ts 10.7 software and professional database [71] as well as ecoinvent 3.8 [72] and AGRIBALYSE [73] LCA databases were used. As the LAC production process took place in Italy, European LCI background datasets from databases were used whenever available.

2.3.3. Life cycle impact assessment and sensitivity analysis

For LCIA the harmonised ReCiPe 2016 q(H) v1.1 methodology [74] was selected, translating the results of the LCI analysis into environmental impacts in two steps. In the step of classification, LCI results are assigned to impact categories, followed by the calculation of category indicator results for each impact category with the help of substance characterization factors. ReCiPe 2016 reports 18 midpoint impact categories [69,74], including climate change, ozone depletion, ecotoxicity, human toxicity, eutrophication or land use, measured through midpoint category indicators (complete list in Table S2 and Table 5). The CO_2 uptake of biomass from the atmosphere during growth was considered as neutral in this study, hence the midpoint category indicator "GWP, excluding biogenic carbon" was selected to represent the midpoint impact category "climate change". The discussion of the LCIA results in this study focuses mainly on climate change (resp. GWP); however, results for all other midpoint impact categories in ReCiPe 2016 are provided as well, with further details made available in the Supplementary Information. A comparison to benchmark AC products in terms of carbon footprint was included in the benchmarking section. In the initial hotspot analysis, the most relevant contributors to LCIA results in the base-case scenario were determined. To assess how indicators for all ReCiPe 2016 [74] midpoint impact categories change, when altering the values of these main contributors, a sensitivity analysis was performed. Values were varied by ±10 %, ±20 % and ±30 % (Fig. S6).

2.3.4. Scenario development and benchmarking

Based on the identified environmental hotspots, several scenarios for process optimization were developed, aiming at the reduction of the environmental impacts of the proposed LAC production process, specifically regarding the midpoint impact category of climate change (resp. GWP). A comparison of the results for the base-case and the best-case LAC scenario to benchmark AC products in terms of carbon footprint is included in the benchmarking section.

3. Results and discussion

In this section the results of the laboratory analyses, as well as of the LCI analysis and the LCIA are presented and critically discussed.

3.1. The pyrolysis process

3.1.1. Analysis of the pyrolysis-activation processes

TGA and bench scale pyrolysis were carried out to understand the effect of pyrolysis conditions on the biochar yield. With regard to TGA, we followed the thermal behaviour of the $KHCO_3$-impregnated biodigestate under a thermal ramp of 5 °C min^{-1}, followed by different isotherm temperatures under argon flow (60 mL min^{-1}). Fig. 1 shows the percentage-weight variation of the $KHCO_3$-impregnated biodigestate over time and temperature. In particular, the temperature was maintained at 800 °C for 60 min (TGA test A), at 900 °C for 60 min (TGA test B) or at 850 °C for 30 min (TGA test C).

The TGA plots clearly show the stages of decomposition during pyrolysis corresponding to a step variation in weight. Up to 800 °C, all TGA profiles exhibit the same trend consisting of several stages. The initial mass loss below 150 °C is mainly related to the removal of moisture [54,55]. At ca. 150 °C the conversion of $KHCO_3$ into K_2CO_3 takes place according to equation (1):

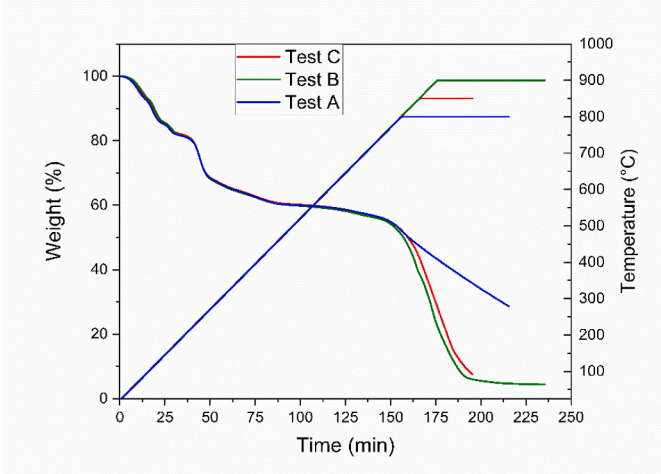

Fig. 1. Weight percentage trends over time and temperature during TGA of $KHCO_3$-impregnated biodigestate under Ar flow for different isotherms: 800 °C for 60 min (blue line, test A), 900 °C for 60 min (green line, test B), and 850 °C for 30 min (red line, test C). (A colour version of this figure can be viewed online.)

$$2\ KHCO_3 \rightarrow K_2CO_3 + CO_2 + H_2O \quad (1)$$

Simultaneously, the main constituents of the biomass, that is, cellulose and hemicellulose (150–400 °C) and lignin (160–900 °C) start to decompose. Above 200 °C up to 750 °C the mass does not change significantly because the main process is the conversion of biomass into carbon. Above 700 °C the sharp mass loss is due to the activation process related to K_2CO_3 decomposition (T > 890 °C, Eq. (2)), carbon burn-off (Eq. (3) and (4)), and carbon gasification (T > 850 °C, Eq. (5)):

$$K_2CO_3 \rightarrow K_2O + CO_2 \quad (2)$$

$$3K_2O + C \rightarrow 4K + K_2CO_3 \quad (3)$$

$$K_2CO_3 + 2C \rightarrow 2K + 3CO \quad (4)$$

$$C + CO_2 \rightarrow 2\ CO \quad (5)$$

According to equations (3) and (4), it is important to keep the system under N_2 over cooling down to 150 °C, to avoid the reaction of metallic potassium (generated during the activation process) with oxygen. Therefore, to fully exploit the $KHCO_3$ activating agent, it is important to reach at least 800 °C. Once achieved 800 °C, different isotherms were performed. TGA test A (isotherm at 800 °C for 60 min) provides the highest biochar-ash residue (28.6 %) because the temperature of 800 °C is not sufficient to complete the activation process, even though the isotherm is maintained for 60 min. Indeed, as mentioned above, carbon burn-off and gasification start above 850° (see Eq. (4) and (5)). On the other hand, TGA test B (isotherm at 900 °C for 60 min) results in a low biochar-ash residue (4.4 %) because the high temperature of 900 °C kinetically favours the activation process and carbon burn-off. Finally, TGA test C (isotherm at 850 °C for 30 min) indicates that the activation process at 850 °C for 30 min is sufficient to complete the activation, maintaining a higher biochar-ash residue with respect to test B (7.6 %).

3.1.2. Activated biochar production

As detailed in the Supplementary Information and shown in Fig. 4, the main steps of the conversion of the lignin-rich biodigestate into activated carbon and the main challenges are.

- **Preparation of biodigestate (washing and drying):** the lignin-rich biodigestate is washed with distilled water and an ethanol-water solution to remove impurities, followed by drying at 80 °C overnight.
- **Impregnation with potassium bicarbonate ($KHCO_3$):** a portion of the dried lignin-source is mixed with an aqueous solution of $KHCO_3$ and dried at 80 °C. This step is essential to ensure the homogeneous distribution of the appropriate mass of activating reagent $KHCO_3$ and the lignin-derived biomass. The $KHCO_3$-to-biomass mass ratio is a key parameter that affects biochar porosity.
- **Pyrolysis/activation:** the pyrolysis step is the core of the process and the most sensitive and challenging part that can affect the resulting specific surface area BET.
- **Deashing process:** the samples are deashed to remove residues and impurities using hydrochloric acid (HCl) treatment. At the laboratory scale, this step is challenging in terms of time and resources, because it uses the highest quantity of water and energy.
- **Drying**: the washed activated carbon is finally dried at 80 °C overnight before further use.

In order to explore the effect of different pyrolysis conditions on the biochar texture, we carried out pyrolysis and activation of the biodigestate by following the 3 conditions simulated by TGA. As described in Section 2.1, all pyrolysis-runs were performed with the same heating ramp (5 °C min^{-1}), followed by isotherms of 850 °C for 30 min for sample B7.1 and B17, 900 °C for 60 min for sample B7.2 850 °C for 30 min for sample B7.1, and 800 °C for 60 min for sample B7.3 (Table 1). After leaching, the carbon yield averaged over different samples was approximately 10 % wt. with respect to raw biodigestate.

TGA analyses under O_2 indicated the presence in the biochar of a residual ash content of ca. 10 %. The morphological and textural properties of the different batches were evaluated by using N_2 adsorption/desorption isotherms at 77 K, SEM-EDS, TEM analyses, Raman Spectroscopy and XRD. SEM images did not highlight any significant differences among the different batches. They all feature 1–10 μm particles with large surface pores (few hundred nanometers wide) (Fig. S1). In addition, they shared almost the same elemental composition (Table S3).

Fig. 2 a)-b) show the N_2 adsorption/desorption isotherms at 77 K and the DFT pore size distributions in terms of the incremental pore volume of the different biochar batches, respectively.

At low relative pressures, the isotherm branches of all batches show sharp adsorption inflections which are indicative of type I materials that are characterized by micropores [75]. However, the presence of a hysteresis loop for all samples at higher relative pressures ($0.45 < P/P0 < 1.0$) indicates that the produced biochars also contain mesopores (type IV material). Moreover, by increasing the pyrolysis temperature from 800 °C (batch B7.3) to 900 °C (batch B7.2), the total adsorbed volume increased. While the shape of the B7.2 (850 °C) isotherm is similar to that of B7.1 and just shifted to higher volumes, the shape of the batch B7.3 was different. Specifically, at the low relative pressures ($p/p^\circ < 0.1$) B7.2 isotherm slope is less steep than that of the other samples. In parallel, at $0.2<p/p^\circ<0.8$, unlike the B7.1 and B7.2 curves, the B7.3 isotherm almost linearly increases. These differences are related to different pore volume distributions, as highlighted by the DFT analyses reported in Fig. 2b and Table 2. Fig. 2b shows that the produced biochars mainly feature micropores and mesopores smaller than 10 nm. The pore volume between 2 and 7 nm increases with temperature. In this range, pore size distribution changes with the increase in pyrolysis temperature, showing a shoulder in sample B7.2 (pyrolysis isotherm 850 °C) that is absent in B7.3 (pyrolysis isotherm 800 °C) and becomes a well-defined peak centred at approximately 3 nm in B7.2 (pyrolysis isotherm 900 °C). The isotherm evolution can be explained by considering that, as explained above, maintaining the temperature above 850 °C for an excessive time increases micropore formation, but also promotes carbon burn-off and gasification, which are responsible for the enlargement of the smaller pores.

Table 2 charts the specific surface area BET (SSA), DFT micropore volume, mesopore volume, and total pore volume ratios of the intensities of the Raman D and G band (I_D/I_G) of the different batches. The

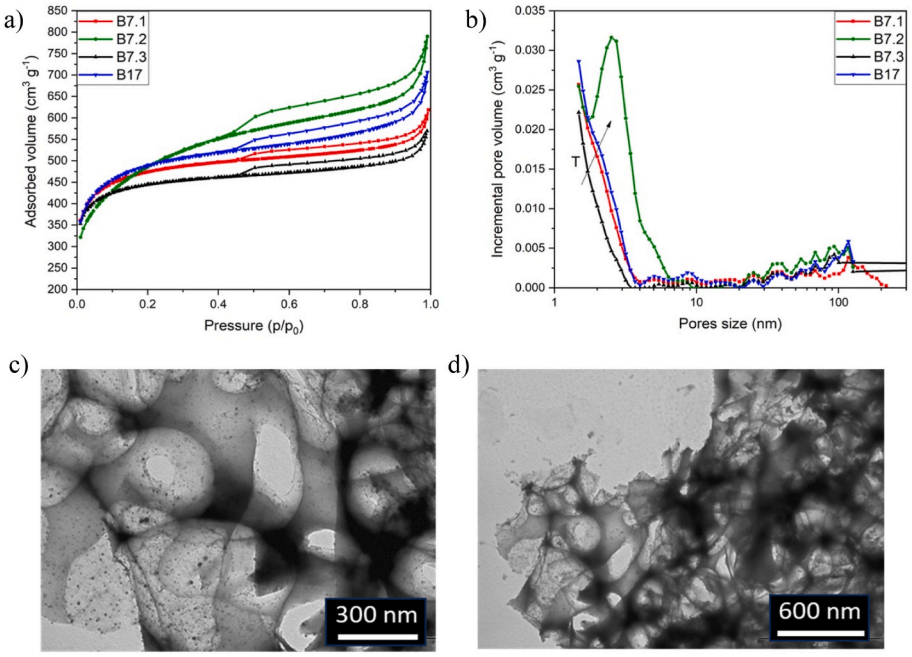

Fig. 2. a) N_2 adsorption/desorption isotherms at 77 K, b) pore size distribution in terms of incremental pore volume of different biochar batches, and c-d) TEM images at different magnifications of sample B7.1. (A colour version of this figure can be viewed online.)

Table 2
Specific surface area (BET) and micropore, mesopore, total pore volumes and ratios of the intensities of the Raman D and G band (I_D/I_G) of the different biochar batches.

Sample	BET Specific area (m^2g^{-1})	Micropore Volume <2 nm (cm^3g^{-1})	Mesopore Volume 2–50 nm (cm^3g^{-1})	Total pore volume (cm^3g^{-1})	I_D/I_G
B7.1 (850 °C)	1806 ± 10	0.564	0.09	0.691 (<217 nm)	0.86
B7.2 (900 °C)	1734 ± 10	0.464	0.26	0.775 (<137 nm)	0.83
B7.3 (800 °C)	1711 ± 10	0.541	0.05	0.621 (<126 nm)	0.80
B17 (850 °C)	1842 ± 10	0.552	0.10	0.693 (<137 nm)	–

highest SSA and micropore volume is achieved by tuning the pyrolysis temperature to 850 °C and reducing the isothermal time from 60 to 30 min. Indeed, the B7.1 biochar exhibited the highest SSA of 1806 $m^2\ g^{-1}$. The B7.1 meso-microporous texture is highlighted by the TEM image reported in Fig. 2(c and d). For B7.2 (900 °C, 1 h) and B7.3 (800 °C, 1 h) SSA resulted 1734 $m^2\ g^{-1}$ and 1711 $m^2\ g^{-1}$, respectively. Interestingly, B7.2 featured the highest total (0.775 $cm^3\ g^{-1}$) and mesopore (0.26 $cm^3\ g^{-1}$) volumes. This confirms that a high pyrolysis temperature improved carbon activation but simultaneously caused the collapse of micropores into larger ones. As expected, B7.3 presents lower pore volumes with respect to B7.1 (see TEM images reported in Fig. S2). Moreover, the I_D/I_G ratio across various batches correlates with their specific surface areas; notably, it increases sequentially from B7.3 to B7.2 and B7.1 [76].

Fig. S3 reports the XR diffraction patterns of the LAC samples that display two broad (002) and (100) reflexes centred at $2\theta = 23°$ and 44°, which are typical for amorphous carbons. These peaks represent the stacking height (Lc) and lateral size of crystallites (La) [77]. As the temperature increases, gradual narrowing of the (002) and widening of the (100) reflections are observed (see Table S4), which correspond to a slight increase of the stacking length (Lc) and a slight reduction in the lateral size (La) of graphitic domains, respectively. The degree of graphitization of activated carbons was evaluated by Raman spectroscopy [76,78–80] and results are reported in Fig. S4 and Table 2. Carbons are characterized by two peaks around 1350 cm^{-1} and 1580 cm^{-1} addressed as D and G bands respectively, which are ascribed to in-plane vibrations of carbons in the sp^2 configuration possessing defects (D) and to in-plane vibrations of carbons in the sp^2 configuration of graphitic materials (G) [81–85]. These bands can be found as two distinct peaks, but in the case of biomass-derived chars, featuring a large amount of amorphous carbon, they overlap. The overlapping region is called V region (Valley) [76]. The ratio between the intensity of the D and G bands can be used to evaluate the amorphous nature of the chars. The ratio of the intensities of the D and G bands (I_D/I_G) reported in Table 2, ranges between 0.83 and 0.88, which is expected for amorphous, high surface area carbons like the lignin-derived activated biochars. Thus, the I_D/I_G ratio of the different batches follows the trend of their specific surface areas, increasing from B7.3 to B7.2 and B7.1 [76].

Overall, the process that provided the best porous architecture of the LAC biochar was pyrolyzed at 850 °C for 30 min (B7.1 and 17). Hence the following section focuses on such selected procedure.

We want to emphasize that employing a real biodigester waste source, which naturally displays variability in composition, could impact both the biochar yield and porosity. A standard deviation of around 4 % was observed for the specific surface area among 14 samples obtained from different source batches. The results presented in this section focus on batches derived from the same washed biodigestate source. This methodology was chosen to minimize variability and more effectively showcase the impact of pyrolysis temperature and duration on carbon yield and porosity.

The electrochemical behaviour of LAC was assessed by a voltametric test run at 10 mV s^{-1} in 6 M KOH. Electrodes with LAC-B17 exhibited

140 ± 10 F g^{-1}, a value that well compares to that of electrodes produced with the commercial carbon PICA BP10 (168 F g^{-1}, with a BET of 1970 m^2 g^{-1}).

3.1.3. Quantitative pyrolysis

The $KHCO_3$-impregnated biodigestate was subjected to bench-scale pyrolysis, which was conducted in the same experimental conditions as the pyrolysis/activation test. This means that the sample was heated (in a nitrogen atmosphere) from RT (25 °C) to 850 °C (maintained for 30 min) with a temperature ramp of 5 °C min^{-1}, while collecting and measuring the evolved pyrolysis products. Accordingly, the biochar fraction was the most abundant product (46 % mass yield) of slow pyrolysis of the impregnated biodigestate, which is in line with literature, followed by the bio-oil fraction with 25 % mass yield. Noticeably, a significant amount (20 % mass yield) of inorganic crystals (tentatively named potash-glass), probably arising from high temperature treatment of $KHCO_3$ in reducing environment, was formed (Fig. 3). Lastly, the pyrolytic gas fraction corresponded to 9 % of the overall mass and was composed of CO, CO_2, H_2, and CH_4 at concentrations of 64 %, 20 %, 13 %, and 3 %, respectively (carrier N_2 gas was excluded). The chemical energy yields were accounted according to the chemical-oxygen demand-based (COD) methods already explained in detail elsewhere [86, 87], obtaining an energy yield of volatile substances of 1.3 and 3.0 MJ kg^{-1} feedstock for bio-oil and syngas fractions, respectively. These values were used to calculate the thermal energy output of combustion of pyrolysis by-products.

3.2. Life cycle assessment

This section provides detailed information on the compilation of the LCI and a discussion of the LCIA results, including a sensitivity analysis. This is followed by scenario development and the discussion of scenario analysis results. The LCA study is finalized by benchmarking with other AC products, a critical discussion of the study's limitations and weaknesses and an outlook regarding further optimization needs and potentials of the here presented LAC production process.

3.2.1. Life cycle inventory

The LCI for the production of LAC in the base-case scenario was compiled based on data obtained from laboratory tests with batch B17, which includes information on process steps, process parameters and consumption of raw materials and auxiliary substances. The laboratory process, which only yielded a few grams of LAC, was up-scaled by applying the framework developed by Piccinno et al. (2016) [57] to a 1000 L reactor (Fig. 4), which would result in a LAC yield of approximately 9 kg per batch (the impregnation step requires the highest reactor volume). The energy consumption for different process steps was adopted from Glogic et al. (2022) [51] and approximated based on Piccinno et al. (2016) [57]. The condensed LCI for the base-case scenario is presented per 1 kg of final product (LAC) in Table 3. More details on single process steps are provided in Table S5. In the base-case scenario, no substance- or energy-recovery and no utilization of pyrolysis by-products were considered and conventional energy sources were applied. Fig. 4 schematizes the flow chart of the LAC-activated carbon production process (B17 batch).

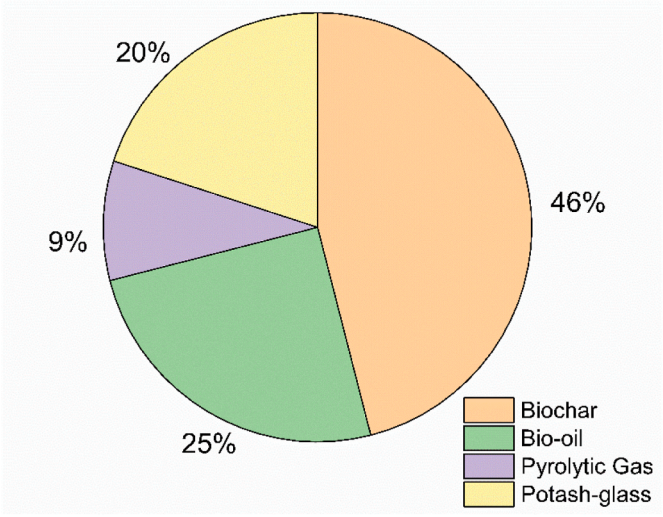

Fig. 3. Mass distribution of pyrolysis products (850 °C for 30 min).

3.2.1.1. Process input. The anaerobic digester plant, which provides the input material for the pyrolysis process, is situated in Italy and fed with maize- and wheat-silage and a small quote of animal manure. The solid waste (biodigestate) is rich in lignin. Suitable LCI datasets for the production of "anaerobic digestate of maize silage" were derived from the French LCA database AGRIBALYSE® [73] (agribalyse_v301_27052021), including biomass-farming, storage in silo, anaerobic digestion and drying of biodigestate to ca. 90 % DM. The corresponding inventories can be found in the Supplementary Information (Tables S6–S8). An LCI dataset for the production of the activating agent potassium bicarbonate ($KHCO_3$) was not readily available in the used LCA databases; therefore, it was modelled following an US patent [88] for the production of $KHCO_3$ from K_2CO_3 and CO_2. Process information as well as the resulting

Table 3
Life cycle inventory for production of 1 kg LAC (base-case scenario, B17 batch, up-scaled).

Process	Value	Unit	Used background process
Input			
Solid digestate from anaerobic digestor ("biodigestate"), ca. 90 % DM	10	kg	Table S8
Ethanol (bio-based)	12.6	kg	Market for ethanol without water 99.7 % solution from fermentation, vehicle grade, CH, ecoinvent 3.8
Potassium bicarbonate ($KHCO_3$)	17	kg	Table S9
Nitrogen	0.6	kg	Nitrogen (gaseous), Sphera, RER
Hydrochloric acid	5	kg	Hydrochloric acid mix (100 %), Sphera, DE
Deionised water	319	kg	Water (deionised), Sphera, RER
Infrastructure	4E-10	units	Market for chemical factory, organics, GLO, ecoinvent 3.8
Electricity	15.4	kWh	Electricity grid mix, RER, Sphera
Heat	109	kWh	Market for heat, district or industrial, natural gas, Europe without Switzerland, ecoinvent 3.8
Transport, lorry	6.96	t km	Lorry transport incl. fuel, Euro 0–6 mix, 22 t total weight, 17.3t max payload, Sphera, RER
Transport, rail	38.6	t km	Rail transport, average train, gross tonne weight 1,000t/726t payload capacity, Sphera, EU-28
Output			
Lignin activated carbon (LAC)	1	kg	
Potassium chloride (KCl)	12	kg	
Syngas (pyrolytic gas)	9.9	kg	
Liquid pyrolysis by-products	6.4	kg	
Potash glass	≥1.6	kg	
Wastewater, to wastewater treatment	128	kg	Waste water treatment (slightly organic and inorganic contaminated), PE, EU-28
of which ethanol	5	kg	
Water to air (emission)	191	kg	
Ethanol to air (emission)	7.7	kg	
Nitrogen to air (emission)	0.6	kg	

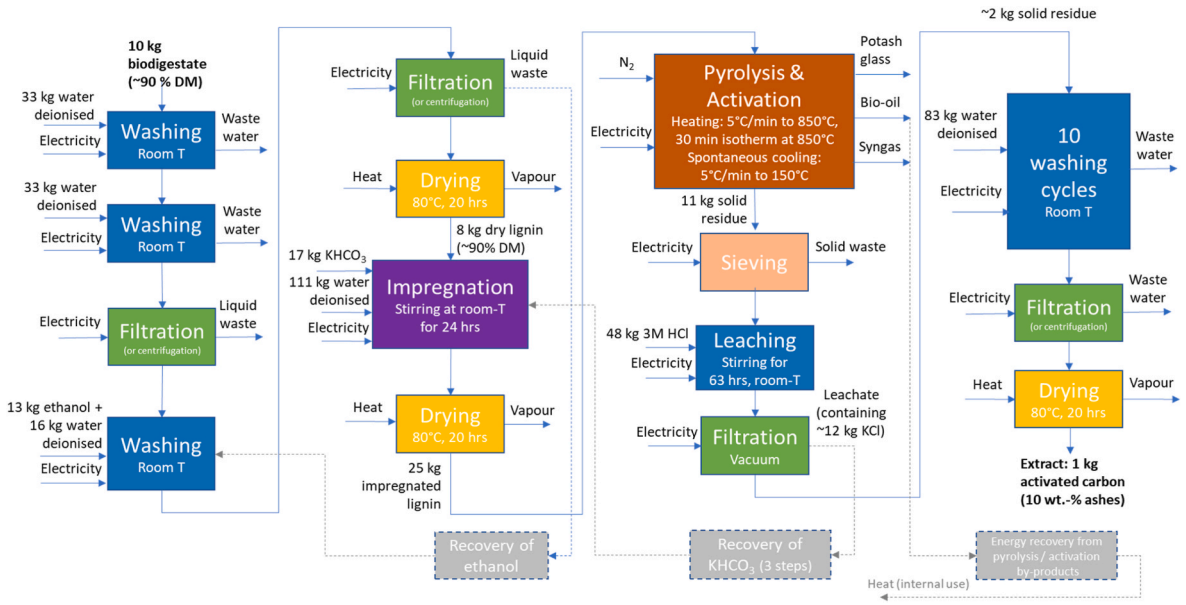

Fig. 4. Flow sheet of LAC production process (B17 batch), up-scaled. (A colour version of this figure can be viewed online.)

LCI to produce 1 kg of potassium bicarbonate can be found in the Supplementary Information (Table S9).

The energy demand for the pyrolysis and activation step was adopted from a publication on supercapacitor electrodes from coconut shell activated carbon [51] and approximated based on the input masses of the processes to compensate for the strongly differing product yields of the cited study and the case presented here. The energy consumption for pumping, mixing, filtration and drying was calculated for a 1000 L reactor by applying the upscaling framework of Piccinno et al. (2016) [57]. The most energy intensive process step in LAC production is drying after impregnation. In contrast to other drying steps in the process, no pre-dewatering (e.g. via filtration, centrifugation) is possible here to avoid loss of the activating agent.

3.2.1.2. Process output. Pyrolysis of lignocellulosic biomass delivers three main products: biochar, syngas and bio-oil. The yields of these three products vary depending on the composition of the biomass (lignin, cellulose and hemicellulose) and the pyrolysis operating parameters [89]. In the present case, a slow pyrolysis (slow heating rate and long residence time) of lignin-rich biomass was performed, resulting in a higher yield of the target product biochar. Syngas and bio-oil can be thermally utilized to provide parts of the required heat for the LAC production process. The amount and energy-content of these pyrolysis by-products was assessed through the quantitative pyrolysis reported in Section 3.1.3.

Originating from $KHCO_3$, K^+ is present in the solid pyrolysis residue as K_2CO_3. In order to remove K^+ from the activated carbon, leaching with hydrochloric acid (HCl) was performed. In this leaching-step potassium chloride (KCl) is formed according to equation (6). The yield of KCl was determined through stoichiometric calculations.

$$2HCl + K_2CO_3 \rightarrow 2\,KCl + H_2O + CO_2 \quad (6)$$

3.2.2. Life cycle impact assessment results and sensitivity analysis

The LCIA of the base-case scenario (hotspot analysis) showed that the production of LAC from anaerobic biodigestate caused a GWP (excl. biogenic carbon) of 63.3 kg CO_2-eq per kg of LAC (Table 5). The main contributors to GWP, as displayed in Fig. 5, were $KHCO_3$, the heat consumption for drying steps, which was supplied by natural gas in the base-case scenario, and ethanol, which was used as a solvent in a washing step before pyrolysis and activation. Details for all other ReCiPe 2016 midpoint impact categories were provided in Fig. S5 of the Supplementary Information. $KHCO_3$ had the highest impacts in most impact categories in the base-case scenario, except for land use, marine eutrophication and ozone depletion. While for climate change (resp. GWP)

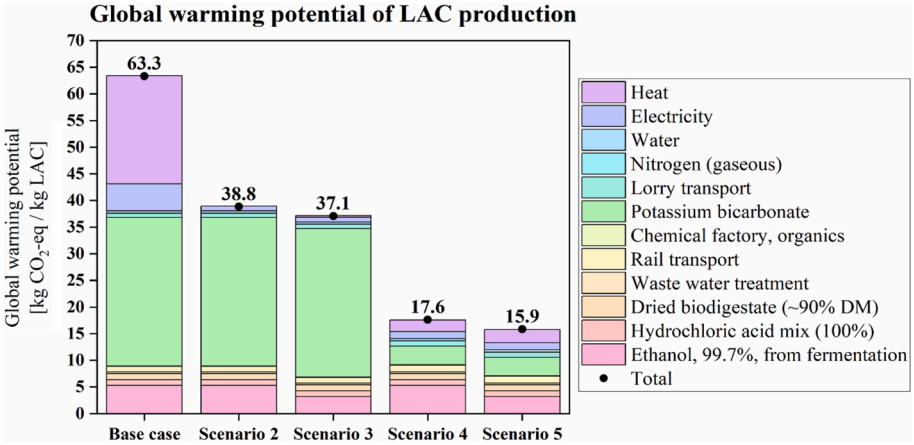

Fig. 5. Global warming potential of production of 1 kg B17–LAC in different scenarios.

the contribution of ethanol, which was used for initial washing of the raw biodigestate, accounted for less than 10 % in the base-case scenario, it was dominant in the three aforementioned categories and also featured a high impact in fine particulate matter formation and terrestrial acidification. Heat, which was supplied by natural gas in the base-case scenario, showed a high impact especially in climate change and fossil depletion, but also in photochemical ozone formation (ecosystems and human health); however, it was not the dominant contributor in any impact category. It can be summarized that the highest impacts in the base-case scenario for all ReCiPe 2016 midpoint impact categories were caused by $KHCO_3$ or by ethanol, followed by heat from natural gas.

A sensitivity analysis was performed by varying the used amounts of these three main contributors. Altering the amount of $KHCO_3$ had a high impact on most impact categories, while changing the consumed heat (from natural gas) specifically targeted climate change and fossil depletion. Varying the amount of ethanol had a major influence on land use, marine eutrophication, photochemical ozone formation (ecosystems and human health), ozone depletion and terrestrial acidification. Details on the sensitivity analysis are provided in S2.3 and Fig. S6 of the Supplementary Information.

3.2.3. Scenario development for LCA

The initial hotspot analysis revealed that the highest potentials for reducing the environmental impacts of the LAC production process lie in the optimization of the use of $KHCO_3$, ethanol and heat. If the primary intention of process optimization was the reduction of GWP, specifically $KHCO_3$ and heat should be targeted, as found in the sensitivity analysis. Based on these insights the optimization scenarios reported in Table 4 were developed. Scenarios 2 to 5 shall demonstrate the effects of substance- and energy-recovery and of the utilization of renewable energy sources on the LCIA results of the LAC production process.

In Scenario 2 energy was recovered from the pyrolysis by-products (syngas and bio-oil) and the remaining energy demand was covered by renewable sources. Assuming a burner efficiency of 80 %, approximately 24 kWh of thermal energy per kg of LAC can be provided to partially supply the heat demand of the process. The remaining 86 kWh of required process heat per kg of LAC (drying steps at 80 °C) were modelled to be provided through a heat pump. A previous work by our group [90] showed that high-temperature heat pumps can reach a coefficient of performance (COP) of 3, which would result in an electricity demand of 29 kWh kg^{-1} of LAC. Options for heat sinks for the heat pump are outside air, process waste heat (waste heat from drying steps) or other available sources of (waste) heat. The heat pump was modelled to be supplied with 100 % renewable electricity (renewable European electricity mix, Table S10).

In Scenario 3 ethanol was recovered through distillation from washing wastewater (filtration step 2) and reused in the LAC production process. The energy demand for distillation was adopted from L. Vane (2008) [91].

In Scenario 4 $KHCO_3$ was recovered from KCl, which was formed during the leaching step, and reused in the LAC production process. The following recovery route is suggested here but has not been verified in the laboratory tests in this project. No loss of K^+ was assumed during activation, pyrolysis and leaching steps. $KHCO_3$ is formed in three steps from KCl, following below equations [88,92–95]:

$$2KCl + 2H_2O \rightarrow 2KOH + Cl_2 + H_2 \quad (7)$$

$$2KOH + CO_2 \rightarrow K_2CO_3 + H_2O \quad (8)$$

$$K_2CO_3 + H_2O + CO_2 \rightarrow 2KHCO_3 \quad (9)$$

The first process step according to equation (7) was modelled with the adapted ecoinvent 3.8 dataset "potassium hydroxide production, RER", which represents the production of KOH through electrolysis of KCl brine [92,93] (Table S11). During electrolysis, the by-products Cl_2 and H_2 are being formed. When producing 1 kg of KOH, approximately 0.63 kg of Cl_2 and 0.02 kg of H_2 are formed according to stoichiometry. However, allocation is already accounted for in the ecoinvent 3.8 dataset, therefore these two by-products are not listed in the LCI (Table S11). The second process step according to equation (8) was modelled with the adapted ecoinvent 3.8 dataset "potassium carbonate production, from potassium hydroxide, GLO" (Table S12) [94,95]. The third process step according to equation (9) is reflected in Table S9 [88]. For the electricity demand a renewable European electricity mix was applied (Table S10) and the additional heat demand was modelled with the Sphera dataset "process steam from biogas 95 %, AT".

Scenario 5 combines all sustainability options from previous scenarios: recovery of $KHCO_3$, recovery of ethanol, energy recovery from pyrolysis by-products and supply of remaining energy demand via 100 % renewable sources.

3.2.4. Scenario analysis results

The results of the optimization of the LAC production process in 4 scenarios for all ReCiPe 2016 impact categories are presented in Table 5. In the best-case scenario (scenario 5), combining all options of energy- and substance-recovery and applying 100 % renewable energy sources in the production process, the GWP (excl. biogenic carbon) of the LAC production could be reduced to 15.9 kg CO_2-eq kg^{-1} LAC. Contributors to GWP in all scenarios are displayed in Fig. 5. For all other ReCiPe 2016 midpoint impact categories further details are provided in Fig. S5 in the Supplementary Information.

There was a reduction in environmental impacts between the base-case scenario and scenario 5 for most impact categories, which can mainly be attributed to the use of 100 % renewable energy sources for the production process, as well as the recovery of the activating agent $KHCO_3$; however, this was not true for land use, which showed a peak in scenario 4. This was mainly caused by the additional heat- and electricity-demand for $KHCO_3$-recovery that was modelled to be provided with 100 % renewable sources, as well as by the use of primary bio-ethanol, which was not recovered in this scenario. Stratospheric ozone depletion and marine eutrophication also showed peaks in scenario 4, for the same reasons as mentioned above; however, a small reduction could be achieved between the base-case scenario and scenario 5. Metal depletion even peaked in scenario 5, which can be attributed to the additional heat demand for $KHCO_3$- and ethanol-recovery. Through recovery of $KHCO_3$ (scenarios 4 and 5), a significant improvement of indicator results in most impact categories could be achieved, including climate change (resp. GWP). The optimization of the energy supply, which was initially applied in scenario 2, strongly reduced the impact values for climate change and for fossil depletion, while the effect on all other impact categories was lower. The recovery of ethanol (scenarios 3 and 5) only had a small positive effect on the GWP and on several other impact categories, while a more distinct effect could be observed on marine eutrophication, stratospheric ozone depletion and terrestrial acidification. Ethanol recovery even deteriorated the impact value for metal depletion. Regarding the impact categories of land use, marine eutrophication, metal depletion and

Table 4
Scenarios for LCA of LAC production process.

Scenario	Description
Base-case scenario	No utilization of by-products, no substance- or energy-recovery, conventional sources of energy (natural gas and European electricity grid mix)
Scenario 2	Energy-recovery from pyrolysis by-products, 100 % renewable sources of energy
Scenario 3	Recovery of ethanol from washing waste-water, energy-recovery from pyrolysis by-products, 100 % renewable sources of energy
Scenario 4	Recovery of $KHCO_3$, energy-recovery from pyrolysis by-products, 100 % renewable sources of energy
Scenario 5	Recovery of ethanol, recovery of $KHCO_3$, energy-recovery from pyrolysis by-products, 100 % renewable sources of energy

Table 5
LCIA results for the production of 1 kg LAC in different scenarios, according to ReCiPe 2016 q(H) v1.1 [74].

Midpoint impact category, ReCiPe2016 [74]	Midpoint category indicator, ReCiPe2016 [74]	Base-case scenario	Scenario 2	Scenario 3	Scenario 4	Scenario 5
Climate change	Global warming potential (GWP), excl. biogenic carbon [kg CO_2-eq]	63.3	38.8	37.1	17.6	15.9
Fine particulate matter formation	Particulate matter formation potential (PMFP) [kg PM2.5-eq]	0.06	0.06	0.06	0.04	0.03
Fossil depletion/fossil resource scarcity	Fossil fuel potential (FFP) [kg oil-eq]	24.5	13.8	13.3	5.1	4.6
Freshwater consumption/water use	Water consumption potential (WCP) [m^3]	0.69	0.67	0.64	0.52	0.49
Freshwater ecotoxicity	Freshwater ecotoxicity potential (FETP) [kg 1,4 DB-eq]	1.28	1.26	1.22	0.26	0.23
Freshwater eutrophication	Freshwater eutrophication potential (FEP) [kg P-eq]	0.016	0.016	0.015	0.004	0.004
Human toxicity, cancer	Human toxicity potential, cancer (HTPc) [kg 1,4-DB-eq]	2.27	2.15	2.06	0.57	0.48
Human toxicity, non-cancer	Human toxicity potential, non-cancer (HTPnc) [kg 1,4-DB-eq]	45.4	45.0	43.3	−1.42	−3.09
Ionizing radiation	Ionizing radiation potential (IRP) [kBq Co-60-eq to air]	6.45	5.96	5.69	1.42	1.15
Land use	Agricultural land occupation potential (LOP) [$m^2 \times$ yr/annual cropland-eq]	15.0	18.7	15.2	28.1	24.5
Marine ecotoxicity	Marine ecotoxicity potential (METP) [kg 1,4-DB-eq]	1.7	1.6	1.6	0.35	0.3
Marine eutrophication	Marine eutrophication potential (MEP) [kg N-eq]	0.017	0.017	0.013	0.020	0.015
Metal depletion/mineral resource scarcity	Surplus ore potential (SOP) [kg Cu-eq]	0.19	0.20	0.22	0.25	0.28
Photochemical ozone formation, ecosystems	Photochemical oxidant formation potential: ecosystems (EOFP) [kg NO_x-eq]	1.64	1.63	1.63	1.62	1.62
Photochemical ozone formation, human health	Photochemical oxidant formation potential: human health (HOFP) [kg NO_x-eq]	1.06	1.05	1.05	1.04	1.04
Ozone depletion	Ozone depletion potential (ODP) [kg CFC-11-eq]	8.3E-05	7.9E-05	6.0E-05	9.5E-05	7.7E-05
Terrestrial acidification	Terrestrial acidification potential (TAP) [kg SO_2-eq]	0.22	0.21	0.18	0.16	0.13
Terrestrial ecotoxicity	Terrestrial ecotoxicity potential (TETP) [kg 1,4-DB-eq]	189.4	188.1	182	45	38.8

stratospheric ozone depletion, which did not exhibit their minimal values in scenario 5, a further optimization of the use of ethanol and, this especially concerns metal depletion, of the heat consumption of the process should be targeted.

Fig. 6 exhibits the energy consumption of the LAC production process in all scenarios. The process step of "drying after impregnation (heat)" showed the highest energy demand. Compared to the base-case scenario, the net-energy-consumption decreased in scenario 2, because of thermal utilization of pyrolysis by-products and supply of residual heat-demand via a heat pump. In scenarios 3 to 5 the net-energy-consumption increased again, due to the additional energy demand for ethanol- (scenario 3) or $KHCO_3$-recovery (scenario 4) or a combination of both (scenario 5).

3.2.5. *Benchmarking*

Comparing LCIA results from this study to benchmark data from literature (Fig. 7), Wang et al. (2022) [62] reported a similar GWP per kilogram of AC. Other sources delivered lower carbon footprints [51, 59–61]. Energy- and water-consumption per kilogram of AC for the production phase were considerably higher in the process presented here than in all cited studies, whereas the product yield (biomass input/AC output) was lower (Table 6).

When comparing LCIA results of different AC products, their intended use, desired physicochemical properties, applied production processes and LCA scope must be considered. AC for use in supercapacitor applications has different quality requirements than AC for soil amendment, fuel or for water-treatment. To meet the required quality criteria of the LAC presented here, a multistage purification process was applied after pyrolysis/activation: sieving, leaching and neutralization, followed by several cycles of washing with water. Grinding of the material was avoided to preserve the highly porous and delicate structure of the LAC. Approximately 11 kg of solid residue obtained directly after pyrolysis/activation resulted in only 1 kg of purified LAC as the final product. In addition, washing and drying before pyrolysis, as well as impregnation and subsequent drying turned out to be very water- and energy-intensive. Wang et al. (2022) [62], who also used a potassium salt (KOH) as activating agent and produced biogenic AC for supercapacitor electrodes, neither described any washing steps before pyrolysis, nor any leaching or further purification steps after pyrolysis. They presented their LCIA results per kg of AC, which, in this case,

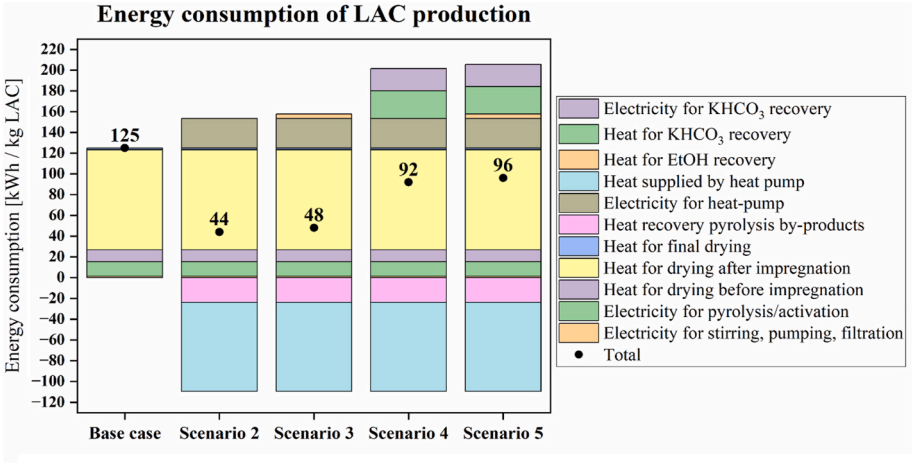

Fig. 6. Energy consumption of production of 1 kg B17–LAC in different scenarios.

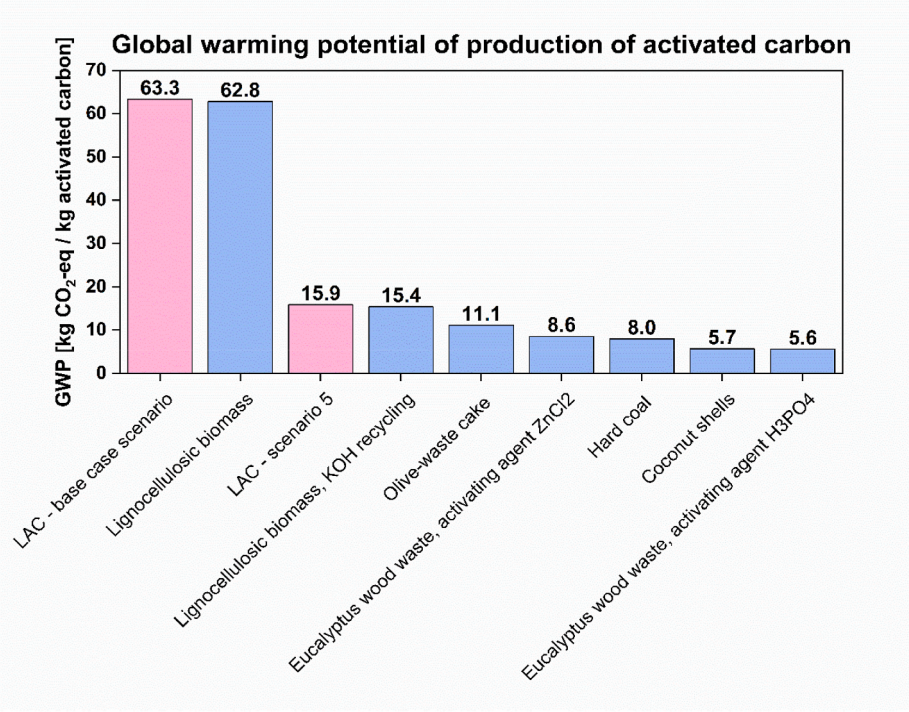

Fig. 7. Global warming potential of production of 1 kg B17-LAC compared to benchmarks: lignocellulosic biomass without and with KOH recycling [62], olive-waste cake [60], eucalyptus wood waste activated by $ZnCl_2$ or H_3PO4 [59], hard coal [58], coconut shells [54]. (A colour version of this figure can be viewed online.)

Table 6
Benchmark for production of activated carbon.

Activated carbon precursor	GWP [kg CO_2eq/ kg AC]	Process scale	LCA scope	Designated use of AC	Mass-ratio dry biomass/ AC	Water consumption in production process [kg/kg AC]	Energy consumption of production process [kWh/kg AC]	Activation agent	Energy or substance recovery?
Hard coal (ecoinvent 3.8) [58]	7.97	Industrial-scale	Cradle-to-gate	Wastewater treatment	3	12.4	5.5	Steam	assumed
Lignocellulosic biomass (energy grasses, woody biomass) [62]	62.78	Industrial-scale (calc.)	Cradle-to-gate	Super-capacitor electrodes	8.9	n.a.	0.67	KOH	no
Lignocellulosic biomass (energy grasses, woody biomass) [62]	15.4	Industrial-scale (calc.)	Cradle-to-gate	Super-capacitor electrodes	8.9	n.a.	0.67	KOH	Recycling of activating agent KOH by 90 %
Olive-waste cake [60]	11.10	Lab-scale	Cradle-to-gate	Not indicated	1.48	8.4	3.1	H_3PO_4	not indicated
Eucalyptus wood waste [59]	8.58	Lab-scale	Gate-to-gate	Not indicated	3.44	10.6	10	$ZnCl_2$	not indicated
Eucalyptus wood waste [59]	5.58	Lab-scale	Gate-to-gate	Not indicated	2.04	9.2	3.89	H_3PO_4	not indicated
Coconut shells [51]	5.68	Industrial-scale (calc.)	Cradle-to-gate	Super-capacitor electrodes	3.65	17.9	5.3	Steam	Energy recovery from pyrolysis-/ activation by-products
LAC - base case scenario	**63.3**	Pilot scale (calc.)	Cradle-to-gate	Super-capacitor electrodes	10	319	125	$KHCO_3$	no
LAC - scenario 5	**15.9**	Pilot scale (calc.)	Cradle-to-gate	Super-capacitor electrodes	10	339	96	$KHCO_3$	Energy and substance recovery, 100 % renewable energy

equaled the mass of solid residue directly after pyrolysis. Hjaila et al. (2013) [60] assessed the environmental impact of AC from olive-waste cake, having no pre-washing of the precursor, but a post-washing, filtration and drying step, which reduced the mass of solid pyrolysis residue from 2.11 kg to 1 kg of final AC. Heidari et al. (2019) [59] also did not describe any pre-washing steps, but a post-washing step with a water consumption of 9.2 kg per kg of AC. Hjaila et al. (2013) [60] and Heidari et al. (2019) [59] found high product yields (ratio input/output) between 1.48 and 3.65, whereas Wang et al. (2022) [62] reported a lower yield of 8.9, which is comparable to the product yield (10) of the

here described process. It is also important to mention that Heidari et al. (2019) [59] performed a gate-to-gate LCA, whereas in all other cited studies on biogenic AC a cradle-to-gate LCA was conducted.

When analyzing these publications on biogenic AC in detail, it is evident that the LCIA results of the cited studies cannot be compared directly to the LAC presented here, particularly due to the high water and energy consumption in the LAC impregnation step and the extensive purification process after LAC pyrolysis/activation, which was not applied in any of the cited studies. Regarding the AC from hard-coal, it must be noted that the ecoinvent dataset for production of "activated carbon from hard-coal" [58] represents optimized and well-proven industrial-scale processes in Europe, resulting in a low GWP of 7.97 kg CO_2-eq per kg of AC. In addition, this hard-coal AC is intended for use in wastewater treatment [58] and not for electrochemical energy storage/conversion applications.

3.2.6. *Limitations of LCA and outlook*

Through LCA of the LAC production process in the base-case scenario, environmental hotspots were identified, which served as the basis for process optimization in scenarios 2 to 5. It has been demonstrated that by applying substance- and energy-recovery and by using renewable sources of energy, the GWP (excl. biogenic carbon) of the LAC production process could be reduced by up to 75 %. Beyond that, further needs and options for process optimization, as well as limitations of this study shall be discussed in this section.

The washing steps, as performed in the LAC laboratory tests, resulted in a very high water consumption per kg of LAC, which was much higher than the benchmark. In an industrial scale process it would be indispensable to drastically reduce the water consumption through an exact evaluation of the necessary water amount, potential selection of alternative washing or purification technologies and water recycling. The process step of impregnating biodigestate with $KHCO_3$ showed a very high energy consumption, as all the water inserted in this step for soaking the biodigestate needed to be removed again through evaporation. This was the most energy intensive step of the LAC production process, resulting in an overall energy consumption that was much higher than the benchmark. An energy-efficient process design, including heat integration, for this step and the entire process, is key to a sustainable and competitive LAC product. Recycling of $KHCO_3$ showed the highest potential for reduction of environmental impacts of the LAC. However, the theoretical recycling process that was described in this study and possible losses of activating agent during LAC production still need to be verified in laboratory tests. The optimization of the required amount of $KHCO_3$ is also of importance. In addition, it would be worth evaluating to what extent compromises in LAC purity (i.e. fewer purification steps) could be tolerated in favour of a better environmental performance of the LAC production process.

For many substances or energy sources, there is more than one dataset available in LCA databases, depending for example on the region of origin, on slightly different material specifications or on other parameters. Thus, special care is required in order to select the most appropriate dataset, as this choice can have a major influence on LCA results. Special caution is also required when comparing a process at a low technology readiness level, such as the one presented here, or to a proven industrial process, such as AC from hard-coal, by means of LCA [56]. Even if upscaling was applied to the LAC laboratory-scale production process and some degree of process optimization was considered, the results cannot exactly reflect real future development due to further research and possible process changes. Nonetheless, it is valuable to get a hint at an early stage on how an emerging process resp. newly proposed product performs compared to benchmark, in order to be able to assess if it might get competitive in the future in terms of sustainability. However, the primary goal of an LCA at an early stage of process development often is the identification of environmental hotspots, hence deriving recommendations for environmentally-targeted process optimization [56], as was demonstrated in this study.

4. Conclusions

In this publication we demonstrate the challenges of employing pyrolysis-activation to produce AC from the lignin-rich solid digestate of a European biodigester plant. We thoroughly analyzed the proposed production process, starting from its study at the laboratory level to conducting a life cyle assessment (LCA). By one-step pyrolysis and activation with $KHCO_3$ it is possible to transform the lignin-rich biodigestate wastes into a valuable product, that is, the lignin-derived high-surface area carbon (LAC) for energy technologies. For such applications, it is of paramount importance to set the proper processing conditions and to follow all the critical steps, including activation and purification, that affect the structural and porous architecture of the resulting biochar.

In our previous research, we illustrated the benefits of utilizing this activated biochar in both supercapacitors and fuel cells. In this study, we have emphasized the challenges associated with scaling up production. While publications on producing high-surface-area carbons from waste for electrochemical energy storage/conversion devices are rapidly increasing, they predominantly focus on the performance of carbon batches prepared at the laboratory scale. Only a few of them critically examine the entire production process to comprehend the environmental impacts of generating significant quantities (kilogram scale) of biochar. To pinpoint any critical stages in the production process, we meticulously followed each phase, while also elucidating the impact of various pyrolysis ramps on carbon quality (evaluated through several analytical techniques), determining carbon production yields (ca. 10 %), and assessing pyrolysis by-products with high energy content, such as bio-oil and syngas.

By pyrolyzing a biodigestate-$KHCO_3$ mixture with a 1:2 mass ratio at 850 °C for 30 min, we obtained the best microporous architecture and the highest specific surface area of 1840 $m^2\ g^{-1}$, which was demonstrated at a 25 g biodigestate batch-scale. This process also delivered pyrolysis by-products with an energy yield of 4.3 MJ kg^{-1} of dried biodigestate impregnated with $KHCO_3$. We observed that increasing the temperature above 850 °C and prolonging pyrolysis time over 30 min improved carbon activation, but simultaneously caused the collapse of micropores into larger ones, with a subsequent decrease in the specific surface area. The best selected procedure was demonstrated from the milligram up to the tens of gram scale, and the outcomes that were gathered from the laboratory scale process study were exploited to assess the sustainability of larger-scale production and to identify its environmentally-targeted optimization routes.

The LCA of the LAC production showed a GWP (excl. biogenic carbon) of 63.3 kg CO_2-eq per kg of LAC in the base-case scenario, using only conventional sources of energy and not applying any substance- or energy-recovery. The activating agent $KHCO_3$, followed by process-heat from conventional sources and ethanol delivered the highest contributions to the overall GWP of the LAC. Based on these findings, several scenarios for process optimization were suggested, resulting in a reduction of the GWP to 15.9 kg CO_2-eq per kg of LAC in the best-case scenario. This still is a higher value than for most cited AC products, including AC from hard coal (7.97 kg CO_2-eq/kg AC); however, these numbers should not lead to premature conclusions. AC from hard-coal is produced in an optimized and well-proven industrial-scale environment in Europe, whereas the LAC presented here features a low technology readiness level. Moreover, the production processes of the cited biogenic AC products do not include extensive purification steps after pyrolysis/activation and have higher product yields than LAC. The targeted high purity and quality of the LAC presented here for use in electrochemical applications must be considered. It is expected that the GWP of the here presented LAC can be further reduced on industrial scale through advanced process optimization and potentially through compromises in LAC purity.

Important aspects and challenges to be considered in the production of LAC from anaerobic biodigestate for electrochemical applications are

i) the low production yield (that is related to the carbon burn-off during the activation step and to the final purification steps), ii) the need of a chemical activating agent, iii) the need of ethanol, of high amounts of water and of deashing processes to ensure high product purity and iii) the increased energy demand, especially for drying steps. However, our study demonstrates that the overall process can be redesigned for better sustainability. We propose to recover $KHCO_3$ from potassium chloride (KCl), which is formed during the leaching step, to recover ethanol from washing wastewater, to thermally utilize the energy-rich pyrolysis by-products and to supply the residual energy demand via renewable sources. Other important challenges in upscaling the proposed LAC production process remain the high water consumption, which would require water purification and recirculation on an industrial scale, as well as the high energy demand, calling for advanced heat integration. These are versatile approaches to be adopted for the design of a sustainable supply chain of supercapacitors and other technologies that require high surface area carbons derived from bio-wastes.

The increasing generation of waste, environmental pollution and rising energy demands that go hand-in-hand with climate change, are among the most pressing global issues today. Harnessing waste materials to produce valuable products can help in addressing these challenges. In our work, we demonstrate that the waste derived from anaerobic biodigester plants can be efficiently utilized as functional materials in technologies aimed at enhancing energy management, such as supercapacitors. This approach allows for the mitigation of challenges posed by the waste-energy nexus and also supports several of the 17 Sustainable Development Goals of the UN. Pyrolysis can be conducted on various biomass sources. However, it is essential to carefully assess the environmental impacts of the applied process as well as its costs. These two factors should guide the method selection.

CRediT authorship contribution statement

Elisabetta Petri: Writing – review & editing, Writing – original draft, Methodology, Investigation, Formal analysis, Data curation, Conceptualization. **Eva-Maria Heigl:** Writing – review & editing, Writing – original draft, Methodology, Investigation, Formal analysis, Data curation, Conceptualization. **Andrea Fasolini:** Writing – review & editing, Writing – original draft, Investigation, Data curation. **Lukas Zeilerbauer:** Formal analysis, Data curation. **Monica Giovannucci:** Writing – review & editing. **Yusuf Küçükağa:** Küçükaga, Writing – review & editing, Writing – original draft, Investigation, Formal analysis, Data curation. **Cristian Torri:** Writing – review & editing, Writing – original draft, Investigation, Formal analysis, Data curation. **Francesco Basile:** Writing – review & editing. **Francesca Soavi:** Writing – review & editing, Supervision, Resources, Project administration, Investigation, Conceptualization.

Declaration of competing interest

The authors declare the following financial interests/personal relationships which may be considered as potential competing interests:

Francesca Soavi reports financial support was provided by European Commission. If there are other authors, they declare that they have no known competing financial interests or personal relationships that could have appeared to influence the work reported in this paper.

Acknowledgements

This project has received funding from the European Union's Horizon 2020 research and innovation programme under grant agreement No. 96355 (HyFlow).

Appendix A. Supplementary data

Supplementary data to this article can be found online at https://doi.org/10.1016/j.carbon.2024.119221.

References

[1] B. Escobar, D.C. Martínez-Casillas, K.Y. Pérez-Salcedo, D. Rosas, L. Morales, S. J. Liao, L.L. Huang, Xuan Shi, Research progress on biomass-derived carbon electrode materials for electrochemical energy storage and conversion technologies, Int. J. Hydrogen Energy 46 (2021) 26053–26073, https://doi.org/10.1016/j.ijhydene.2021.02.017.

[2] L. Suárez, T.A. Centeno, Unravelling the volumetric performance of activated carbons from biomass wastes in supercapacitors, J. Power Sources 448 (2020) 227413, https://doi.org/10.1016/j.jpowsour.2019.227413.

[3] T. Kan, V. Strezov, T.J. Evans, Lignocellulosic biomass pyrolysis: a review of product properties and effects of pyrolysis parameters, Renew. Sustain. Energy Rev. 57 (2016) 1126–1140, https://doi.org/10.1016/j.rser.2015.12.185.

[4] K. Mensah-Darkwa, C. Zequine, P.K. Kahol, R.K. Gupta, Supercapacitor energy storage device using biowastes: a sustainable approach to green energy, Sustainability 11 (2019) 414–436, https://doi.org/10.3390/su11020414.

[5] Z. Gao, Y. Zhang, N. Song, X. Li, Biomass-derived renewable carbon materials for electrochemical energy storage, Materials Research Letters 5 (2017) 69–88, https://doi.org/10.1080/21663831.2016.1250834.

[6] K. Fic, A. Platek, J. Piwek, E. Frackowiak, Sustainable materials for electrochemical capacitors, Mater. Today 21 (2018) 437–454, https://doi.org/10.1016/j.mattod.2018.03.005.

[7] S. Sharma, S. Basu, N.P. Shetti, M. Kamali, P. Walvekar, Tejraj M. Aminabhavi, Waste-to-energy nexus: a sustainable development, Environ. Pollut. 267 (2020) 115501, https://doi.org/10.1016/j.envpol.2020.115501.

[8] The 17 Sustainable Development Goals (SDGs) of the United Nations, https://sdgs.un.org/goals.

[9] N.A. Rashidi, Y.H. Chai, I.S. Ismail, M.F.H. Othman, S. Yusup, Biomass as activated carbon precursor and potential in supercapacitor applications, Biomass Conversion and Biorefinery (2022), https://doi.org/10.1007/s13399-022-02351-1.

[10] European Commission - Joint Research Centre - Institute for Environment and Sustainability: *International Reference Life Cycle Data System (ILCD) Handbook - General guide for Life Cycle Assessment - Detailed guidance*, first ed., Publications Office of the European Union, Luxembourg, 2010. March 2010. EUR 24708 EN, https://eplca.jrc.ec.europa.eu/uploads/ILCD-Handbook-General-guide-for-LCA-DETAILED-GUIDANCE-12March2010-ISBN-fin-v1.0-EN.pdf.

[11] L.J. Müller, A. Kätelhön, M. Bachmann, A. Zimmermann, A. Sternberg, A. Bardow, *A Guideline for life cycle Assessment of carbon Capture and utilizatio*n, Front. Energy Res. 8 (2020). Article 15, https://www.frontiersin.org/articles/10.3389/fenrg.2020.00015/full.

[12] P. Thangavel, G. Kim, K.S. Kim, *Electrochemical integration of amorphous NiFe (oxy) hydroxides on surface-activated carbon fibers for high-efficiency oxygen evolution in alkaline anion exchange membrane water electrolysis*, J. Mater. Chem. A 9 (2021) 14043–14051, https://doi.org/10.1039/D1TA02883A.

[13] M. Serafini, F. Mariani, A. Fasolini, E. Scavetta, F. Basile, D. Tonelli, *Nanostructured copper-based electrodes electrochemically Synthesized on a carbonaceous gas diffusion Membrane with catalytic Activity for the Electroreduction of CO_2*, ACS Appl. Mater. Interfaces 13 (2021) 57451–57461, https://doi.org/10.1021/acsami.1c18844.

[14] G. Zini, R. Marazzi, S. Pedrazzi, P. Tartarini, A solar hydrogen hybrid system with activated carbon storage, Int. J. Hydrogen Energy 35 (2010) 4909–4917, https://doi.org/10.1016/j.ijhydene.2009.09.014.

[15] X. Zhao, X. Yong, Q. Ji, Z. Yang, Y. Song, Y. Sun, Z. Cai, J. Xu, L. Li, S. Shi, F. Chen, C. Li, P. Wang, J. Baek, Controlled synthesis of highly active bifunctional electrocatalysts for overall water splitting using coal-based activated carbons, J. Mater. Chem. A 11 (2023) 12726–12734, https://doi.org/10.1039/D2TA06595A.

[16] Y.S. Park, J. Jeong, Y. Noh, M.J. Jang, J. Lee, K.H. Lee, D.C. Lim, M.H. Seo, W. B. Kim, J. Yang, S.M. Choi, Commercial anion exchange membrane water electrolyzer stack through non-precious metal electrocatalysts, Appl. Catal. B Environ. 292 (2021) 120170, https://doi.org/10.1016/j.apcatb.2021.120170.

[17] B. Escobar, D.C. Martínez-Casillas, K.Y. Pérez-Salcedo, D. Rosas, L. Morales, S. J. Liao, L.L. Huang, Xuan Shi, Research progress on biomass-derived carbon electrode materials for electrochemical energy storage and conversion technologies, Int. J. Hydrogen Energy 46 (2021) 26053–26073, https://doi.org/10.1016/j.ijhydene.2021.02.017.

[18] A.S. Mestre, A.P. Carvalho, *Nanoporous carbon synthesis: an old Story with exciting new chapters*, porosity - process, Technologies and Applications (2017) 37–68, https://doi.org/10.5772/intechopen.72476.

[19] K.T. Idris-Hermann, T.T. Donald Raoul, D. Giscard, A. Solomon Gabche, Preparation and characterization of activated carbons from bitter kola (Garcinia kola) nut shells by chemical activation method using H_3PO_4; KOH and $ZnCl_2$, Chemical Science International Journal 23 (2018) 1–15, https://doi.org/10.9734/CSJI/2018/43411.

[20] L. Jiang, L. Sheng, Z. Fan, Biomass-derived carbon materials with structural diversities and their applications in energy storage, Sci. China Mater. 61 (2018) 133–158, https://doi.org/10.1007/s40843-017-9169-4.

[21] J.A. Sosa, J.R. Laines, D.S. García, R. Hernández, M. Zappi, A.E.E. Monteros, Activated carbon: a review of residual precursors, synthesis processes, characterization techniques, and applications in the improvement of biogas, Environmental Engineering Research 28 (2023), https://doi.org/10.4491/eer.2022.100.

[22] X. Zhang, M. Tu, M.G. Paice, Routes to potential bioproducts from lignocellulosic biomass lignin and hemicelluloses, BioEnergy Research 4 (2011) 246–257, https://doi.org/10.1007/s12155-011-9147-1.

[23] A. Fasolini, R. Cucciniello, E. Paone, F. Mauriello, T. Tabanelli, A short overview on the hydrogen production via aqueous phase reforming (APR) of cellulose, C6-C5 sugars and polyols, Catalysts 9 (2019) 917, https://doi.org/10.3390/catal9110917.

[24] R. Kandiyoti, A. Herod, K. Bartle, T. Morgan, Solid Fuels and Heavy Hydrocarbon Liquids, second ed., Elsevier, 2017 https://doi.org/10.1016/B978-0-08-100784-6.00010-2.

[25] W. Liu, H. Jiang, H. Yua, Thermochemical conversion of lignin to functional materials: a review and future directions, Green Chemistry 17 (2015) 4888–4907, https://doi.org/10.1039/C5GC01054C.

[26] J. Mumme, L. Eckervogt, J. Pielert, M. Diakité, F. Rupp, J. Kern, Hydrothermal carbonization of anaerobically digested maize silage, Bioresour. Technol. 102 (2011) 9255–9260, https://doi.org/10.1016/j.biortech.2011.06.099.

[27] F. Almomani, R.R. Bhosale, Enhancing the production of biogas through anaerobic co-digestion of agricultural waste and chemical pre-treatments, Chemosphere 255 (2020) 126805, https://doi.org/10.1016/j.chemosphere.2020.126805.

[28] A.R. Sahito, R.B. Mahar, F. Ahmed, Optimization of organic loading rate and hydraulic retention time for maximum production of methane through anaerobic co- digestion of canola straw and buffalo dung, The Journal of Animal & Plant Sciences 26 (2016) 373–381.

[29] E. Gul, K.A.B. Alrawashdeh, O. Masek, Ø. Skreiberg, A. Corona, M. Zampilli, L. Wang, P. Samaras, Q. Yang, H. Zhou, P. Bartocci, F. Fantozzi, Production and use of biochar from lignin and lignin-rich residues (such as digestate and olive stones) for wastewater treatment, J. Anal. Appl. Pyrol. 158 (2021) 105263, https://doi.org/10.1016/j.jaap.2021.105263.

[30] D.S. Bajwa, G. Pourhashem, A.H. Ullah, S.G. Bajwa, A concise review of current lignin production, applications, products and their environmental impact, Ind. Crop. Prod. 139 (2019) 111526, https://doi.org/10.1016/j.indcrop.2019.111526.

[31] I. Haq, P. Mazumder, A.S. Kalamdhad, Recent advances in removal of lignin from paper industry wastewater and its industrial applications – a review, Bioresour. Technol. 312 (2020) 123636, https://doi.org/10.1016/j.biortech.2020.123636.

[32] Z. Bi, Q. Kong, Y. Cao, G. Sun, F. Su, X. Wei, X. Li, A. Ahmad, L. Xie, C.M. Chen, Biomass-derived porous carbon materials with different dimensions for supercapacitor electrodes: a review, J. Mater. Chem. A 7 (2019) 16028, https://doi.org/10.1039/c9ta04436a.

[33] J.I. Hayashi, A. Kazehaya, K. Muroyama, A.P. Watkinson, Preparation of activated carbon from lignin by chemical activation, Carbon 38 (2000) 1873–1878, https://doi.org/10.1016/S0008-6223(00)00027-0.

[34] J.W. Jeon, L. Zhang, J.L. Lutkenhaus, D.D. Laskar, J.P. Lemmon, D. Choi, M. I. Nandasiri, A. Hashmi, J. Xu, R.K. Motkuri, Controlling porosity in lignin-derived nanoporous carbon for supercapacitor applications, Chemistry Sustainability Energy Materials 8 (2015) 428–432, https://doi.org/10.1002/cssc.201402621.

[35] D. Saha, Y. Li, Z. Bi, J. Chen, J.K. Keum, D.K. Hensley, H.A. Grappe, H.M. Meyer III, S. Dai, M.P. Paranthaman, Studies on supercapacitor electrode material from activated lignin-derived mesoporous carbon, Langmuir 30 (2014) 900–910, https://doi.org/10.1021/la404112m.

[36] A.M. Navarro-Suárez, J. Carretero-González, V. Roddatis, E. Goikolea, J. Ségalini, E. Redondo, T. Rojo, R. Mysyk, Nanoporous carbons from natural lignin: study of structural–textural properties and application to organic-based supercapacitors, RSC Adv. 4 (2014) 48336, https://doi.org/10.1039/C4RA08218D.

[37] B. Moyo, D. Momodu, O. Fasakin, A. Bello, J. Dangbegnon, N. Manyala, Electrochemical analysis of nanoporous carbons derived from activation of polypyrrole for stable supercapacitors, J. Mater. Sci. 53 (2018) 5229–5241, https://doi.org/10.1007/s10853-017-1911-y.

[38] B.K. Mutuma, N.F. Sylla, A. Bubu, N.M. Ndiaye, C. Santoro, A. Brilloni, F. Poli, N. Manyala, F. Soavi, Valorization of biodigestor plant waste in electrodes for supercapacitors and microbial fuel cells, Electrochim. Acta 391 (2021) 138960, https://doi.org/10.1016/j.electacta.2021.138960.

[39] M. Muhyuddin, A. Friedman, F. Poli, E. Petri, H. Honig, F. Basile, A. Fasolini, R. Lorenzi, E. Berretti, M. Bellini, A. Lavacchi, L. Elbaz, C. Santoro, F. Soavi, Lignin-derived bimetallic platinum group metal-free oxygen reduction reaction electrocatalysts for acid and alkaline fuel cells, J. Power Sources 556 (2023) 232416, https://doi.org/10.1016/j.jpowsour.2022.232416.

[40] P.J.M. Carrott Suhas, M.M.L. Ribeiro Carrott, Lignin – from natural adsorbent to activated carbon: a review, Bioresour. Technol. 98 (2007) 2301–2312, https://doi.org/10.1016/j.biortech.2006.08.008.

[41] K. Chen, Z. He, Z. Liu, A.J. Ragauskas, B. Li, Y. Yuan, Emerging modification technologies of lignin-based activated carbon toward advanced applications, Chemistry Sustainability Energy Materials 15 (2022), https://doi.org/10.1002/cssc.202201284.

[42] Regulation (EC) No 1272/2008 of the European Parliament and of the Council of 16 December 2008 on classification, labelling and packaging of substances and mixtures, amending and repealing Directives 67/548/EEC and 1999/45/EC, and amending Regulation (EC) No 1907/2006, https://eur-lex.europa.eu/eli/reg/2008/1272/oj.

[43] N. Sylla, N. Ndiaye, B. Ngom, D. Momodu, M. Madito, B. Mutuma, N. Manyala, Effect of porosity enhancing agents on the electrochemical performance of high-energy ultracapacitor electrodes derived from peanut shell waste, Sci. Rep. 9 (2019) 13673, https://doi.org/10.1038/s41598-019-50189-x.

[44] M. Sevilla, A.B. Fuertes, A green approach to high-performance supercapacitor electrodes: the chemical activation of hydrochar with potassium bicarbonate, Chemistry Sustainability Energy Materials 9 (2016) 1880–1888, https://doi.org/10.1002/cssc.201600426.

[45] J. Sahira, A. Mandira, P.B. Prasad, P.R. Ram, Effects of activating agents on the activated carbons prepared from lapsi seed stone, Res. J. Chem. Sci. 3 (2013) 19–24.

[46] Y. Xi, D. Yang, X. Qiu, H. Wang, J. Huang, Q. Li, Renewable lignin-based carbon with a remarkable electrochemical performance from potassium compound activation, Industrial Crops and Products 124 (2018) 747–754, https://doi.org/10.1016/j.indcrop.2018.08.018.

[47] F.O. Ochai-Ejeh, D.Y. Momodu, M.J. Madito, A.A. Khaleed, K.O. Oyedotun, S. C. Ray, N. Manyala, Nanostructured porous carbons with high rate cycling and floating performance for supercapacitor application, AIP Advaces 8 (2018) 055208, https://doi.org/10.1063/1.5023046.

[48] D. Momodu, N.F. Sylla, B. Mutuma, A. Bello, T. Masikhwa, S. Lindberg, A. Matic, N. Manyala, Stable ionic-liquid-based symmetric supercapacitors from Capsicum seed-porous carbons, J. Electroanal. Chem. 838 (2019) 119–128, https://doi.org/10.1016/j.jelechem.2019.02.045.

[49] F. Poli, D. Momodu, G.E. Spina, A. Terella, B.K. Mutuma, M.L. Focarete, N. Manyala, F. Soavi, Pullulan-ionic liquid-based supercapacitor: a novel, smart combination of components for an easy-to-dispose device, Electrochim. Acta 338 (2020) 135872, https://doi.org/10.1016/j.electacta.2020.135872.

[50] F. Poli, C. Santoro, F. Soavi, Improving microbial fuel cells power output using internal and external optimized, tailored and totally green supercapacitor, J. Power Sources 564 (2023) 232780, https://doi.org/10.1016/j.jpowsour.2023.232780.

[51] E. Glogic, A.K. Kamali, N.M. Keppetipola, B. Alonge, G.R.A. Kumara, G. Sonnemann, T. Toupance, L. Cojocaru, Life cycle assessment of supercapacitor electrodes based on activated carbon from coconut shells, ACS Sustain. Chem. Eng. 10 (2022) 15025–15034, https://doi.org/10.1021/acssuschemeng.2c03239.

[52] International Energy Agency, Outlook for Biogas and Prospects for Organic Growth World Energy Outlook Special Report Biomethane, IEA, 2020. https://iea.blob.core.windows.net/assets/03aeb10c-c38c-4d10-bcec-de92e9ab815f/Outlook_for_biogas_and_biomethane.pdf.

[53] HyFlow, Development of a sustainable hybrid storage system based on high power vanadium redox flow battery and supercapacitor-technology, European Union's Horizon 2020 research and innovation programme under grant agreement No 963550, https://hyflow-h2020.eu/.

[54] Y. Wongmat, D.R. Wagner, Effect of potassium salts on biochar pyrolysis, Energies 15 (16) (2022) 5779, https://doi.org/10.3390/en15165779.

[55] A.K. Sakhiya, A. Anand, P. Kaushal, Production, activation, and applications of biochar in recent times, Biochar (2) (2020) 253–285, https://doi.org/10.1007/s42773-020-00047-1.

[56] S. Cucurachi, B. Steubing, F. Siebler, N. Navarre, C. Caldeira, S.P. Sala, Prospective LCA Methodology for Novel and Emerging Technologies for BIO-Based Products - the Planet Bio Project, publications Office of the European Union, Luxembourg, 2022, https://doi.org/10.2760/167543. JRC129632.

[57] F. Piccinno, R. Hischier, S. Seeger, C. Som, From laboratory to industrial scale: a scale-up framework for chemical processes in life cycle assessment studies, J. Clean. Prod. 135 (2016) 1085–1097, https://doi.org/10.1016/j.jclepro.2016.06.164.

[58] Ecoinvent. 3.8, *Dataset: Activated carbon production, granular from hard coal*, RER, https://ecoquery.ecoinvent.org/3.9.1/cutoff/dataset/15255/export.

[59] A. Heidari, E. Khaki, H. Younesi, H.R. Lu, Evaluation of fast and slow pyrolysis methods for bio-oil and activated carbon production from eucalyptus wastes using a life cycle assessment approach, J. Clean. Prod. 241 (2019) 118394, https://doi.org/10.1016/j.jclepro.2019.118394.

[60] K. Hjaila, R. Baccar, M. Sarrà, C.M. Gasol, P. Blánquez, Environmental impact associated with activated carbon preparation from olive-waste cake via life cycle assessment, J. Environ. Manag. 130 (2013) 242–247, https://doi.org/10.1016/j.jenvman.2013.08.061.

[61] V. Montes, J.M. Hill, Activated carbon production: recycling KOH to minimize waste, Mater. Lett. 220 (2018) 238–240, https://doi.org/10.1016/j.matlet.2018.03.019.

[62] Y. Wang, J. Wang, X. Zhang, D. Bhattacharyya, E.M. Sabolsky, Quantifying environmental and economic impacts of highly porous activated carbon from lignocellulosic biomass for high-performance supercapacitors, Energies 15 (2022) 351, https://doi.org/10.3390/en15010351.

[63] Y. Küçükağa, A Novel Hybrid Thermochemical-Biological Refinery Integrated with Power-To-X Technology for Obtaining Biopolymers, Alma Mater Studiorum Università di Bologna, 2023. PhD Thesis in Chemistry at, http://amsdottorato.unibo.it/10547/.

[64] A. Facchin, K. Yusuf, D. Fabbri, C. Torri, Analytical evaluation of the coupling of hydrothermal carbonization and pyrolysis (HTC-Py) for the obtainment of bioavailable products, J. Anal. Appl. Pyrol. 175 (2023) 106185, https://doi.org/10.1016/j.jaap.2023.106185.

[65] International Organization for Standardization, ISO 14040:2006(en). Environmental management - Life cycle assessment - Principles and framework. https://www.iso.org/obp/ui#iso:std:iso:14040:ed-2:v1:en, 2006.

[66] International Organization for Standardization, ISO 14044:2006(en). Environmental management - Life cycle assessment - Requirements and guidelines. https://www.iso.org/obp/ui#iso:std:iso:14044:ed-1:v1:en, 2006.

[67] R. Frischknecht, Lehrbuch der Ökobilanzierung, Springer Spektrum, Berlin, 2020, https://doi.org/10.1007/978-3-662-54763-2. ISBN 978-3-662-54762-5, ISBN 978-3-662-54763-2 (eBook).
[68] J.B. Guinée, M. Gorrée, R. Heijungs, G. Huppes, R. Kleijn, A. Koning, L.- de, van Oers, A. Wegener Sleeswijk, S. Suh, H.A. Udo de Haes, H. Bruijn, R. van Duin, M. Huijbregts, in: Handbook on Life Cycle Assessment. Operational Guide to the ISO Standards, first ed., Springer, Dordrecht, Dordrecht, 2002. ISBN : 978-1-4020-0228-1, https://link.springer.com/book/10.1007/0-306-48055-7.
[69] M.A. Curran (Ed.), Life Cycle Assessment Handbook. A Guide for Environmentally Sustainable Products, Wiley, 2012, https://doi.org/10.1002/9781118528372. Print-ISBN: 9781118099728, Online-ISBN: 9781118528372, https://onlinelibrary.wiley.com/doi/book/10.1002/9781118528372.
[70] W. Klöpffer, B. Grahl, *Life Cycle Assessment (LCA)*. A Guide to Best Practice, Wiley-VCH, Weinheim, Germany, 2014. ISBN: 978-3-527-65564-9.
[71] Sphera Solutions Inc, Sphera - environmental database. GaBi Professional Database, 2023. https://sphera.com/product-sustainability-gabi-data-search/.
[72] Ecoinvent Association, Ecoinvent 3.8 - Environmental Database, 2023. https://ecoinvent.org/.
[73] AGRIBALYSE, AGRIBALYSE®. French LCA Database, Focussing on Agriculture and Food Production, 2023. https://doc.agribalyse.fr/documentation-en/.
[74] M.A.J. Huijbregts, Z.J.N. Steinmann, P.M.F. Elshout, G. Stam, F. Verones, M. Vieira, M. Zijp, A. Hollander, R. van Zelm, ReCiPe2016: a harmonised life cycle impact assessment method at midpoint and endpoint level, The International Journal of Cycle Life Assessment 22 (2017) (2017) 138–147, https://doi.org/10.1007/s11367-016-1246-y.
[75] S. Brunauer, P.H. Emmet, E. Teller, Adsorption of gases in multimolecular layer, J. Am. Chem. Soc. 60 (1938) 309–319. https://pubs.acs.org/doi/abs/10.1021/ja01269a023.
[76] C. Guizani, M. Jeguirim, S. Valin, L. Limousy, S. Salvador, Biomass chars: the effects of pyrolysis conditions on their morphology, structure, chemical properties and reactivity, Energies 10 (2017) 796, https://doi.org/10.3390/en10060796.
[77] B.S. Girgis, Y.M. Temerk, M.M. Gadelrab, I.D. Abdullah, X-Ray diffraction patterns of activated carbons prepared under various conditions, Carbon letters 8 (2007) 95–100, https://doi.org/10.5714/CL.2007.8.2.095.
[78] C. Guizani, K. Haddad, L. Limousy, M. Jeguirim, New insights on the structural evolution of biomass char upon pyrolysis as revealed by the Raman spectroscopy and elemental analysis, Carbon 119 (2017) 519–521, https://doi.org/10.1016/j.carbon.2017.04.078.
[79] M.W. Smith, I. Dallmeyer, T.J. Johnson, C.S. Brauer, J. McEwen, J.F. Espinal, M. Garcia-Perez, Structural analysis of char by Raman spectroscopy: improving band assignments through computational calculations from first principles, Carbon 100 (2016) 678–692, https://doi.org/10.1016/j.carbon.2016.01.031.
[80] L. Bokobza, J. Bruneel, M. Couzi, Raman Spectra of Carbon-Based Materials (From Graphite to Carbon Black) and of Some Silicone Composites, C, vol. 1, 2015, pp. 77–94.
[81] A.C. Ferrari, J. Robertson, Interpretation of Raman spectra of disordered and amorphous carbon, Phys. Rev. B 61 (2000) 14095–14107, https://doi.org/10.1103/PhysRevB.61.14095.
[82] L.G. Cançado, A. Jorio, E.H.M. Ferreira, F. Stavale, C.A. Achete, R.B. Capaz, M.V. O. Moutinho, A. Lombardo, T.S. Kulmala, A.C. Ferrari, Quantifying defects in graphene via Raman spectroscopy at different excitation energies, Nano Lett. 11 (2011) 3190–3196, https://doi.org/10.1021/nl201432g.
[83] C. Casimero, C. Hegarty, R.J. McGlynn, J. Davis, Ultrasonic exfoliation of carbon fiber: electroanalytical perspectives, J. Appl. Electrochem. 50 (2020) 383–394, https://doi.org/10.1007/s10800-019-01379-y.
[84] B.J. Matsoso, K. Ranganathan, B.K. Mutuma, T. Lerotholi, G. Jones, N.J. Coville, Time-dependent evolution of the nitrogen configurations in N-doped graphene films, RSC Adv. 6 (2016) 106914–106920, https://doi.org/10.1039/C6RA24094A, 106914-106920.
[85] L.M. Malard, M.A. Pimenta, G. Dresselhaus, M.S. Dresselhaus, Raman spectroscopy in graphene, Phys. Rep. 473 (2009) 51–87.
[86] C. Torri, L. Favaro, A. Facchin, Y. Küçükağa, A.G. Rombolà, D. Fabbri, Could pyrolysis substitute hydrolysis in 2nd generation biomass valorization strategies? A chemical oxygen demand (COD) approach, J. Anal. Appl. Pyrol. 163 (2022) 105467, https://doi.org/10.1016/j.jaap.2022.105467.
[87] Y. Küçükağa, A. Facchin, S. Kara, T.Y. Nayır, D. Scicchitano, S. Rampelli, M. Candela, C. Torri, Conversion of pyrolysis products into volatile fatty acids with a biochar-packed anaerobic bioreactor, Ind. Eng. Chem. Res. 61 (2022) 16624–16634, https://doi.org/10.1021/acs.iecr.2c02810.
[88] A. D. Kurtz, A. E. Winston, Process for the Production of Potassium Bicarbonate". *US patent no. 4,919,910A*, 1988, US4919910A - Process for the production of potassium bicarbonate - Google Patents.
[89] D. Gahane, D. Biswal, S.A. Mandavgane, Life cycle assessment of biomass pyrolysis, BioEnergy Research 15 (2022) 1387–1406, https://doi.org/10.1007/s12155-022-10390-9.
[90] L. Zeilerbauer, F. Hubmann, S. Puschnigg, J. Lindorfer, Life cycle assessment and shadow cost of steam produced by an industrial-sized high-temperature heat pump, Sustain. Prod. Consum. 40 (2023) 48–62, https://doi.org/10.1016/j.spc.2023.06.016.
[91] L.M. Vane, Separation technologies for the recovery and dehydration of alcohols from fermentation broths, Bio: Biofuels, Bioproducts & Biorefining 2 (2008) 550–588, https://doi.org/10.1002/bbb.108.
[92] Ecoinvent 3.8, Dataset: Potassium hydroxide production, potassium hydroxide, RER, 1998-2023, https://ecoquery.ecoinvent.org/3.9.1/cutoff/dataset/7310/documentation.
[93] N. Jungbluth, et al., Life Cycle Inventories of Bioenergy. Ecoinvent Report No. 17. Data v.2.0, Swiss Centre for Life Cycle Inventories., Uster, December 2007. https://db.ecoinvent.org/reports/17_bioenergy.pdf.
[94] Ecoinvent 3.8, Dataset: Potassium carbonate production, from potassium hydroxide, RER, 2003-2023., https://ecoquery.ecoinvent.org/3.9.1/cutoff/dataset/5977/documentation.
[95] J. Sutter, Life cycle inventories of highly pure chemicals, data v2.0 (2007), *ecoinvent report No. 19*, Uster, https://db.ecoinvent.org/reports/08_Chemicals.pdf, December 2007.